Cosmological Signal & Image Processing

Jason McEwen
www.jasonmcewen.org
@jasonmcewen

Mullard Space Science Laboratory (MSSL)
University College London (UCL)

Cosmology @ MSSL

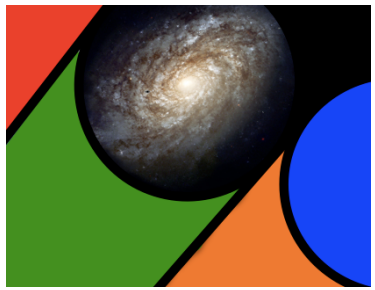

Australian National University (ANU), March 2014

LSS fly through

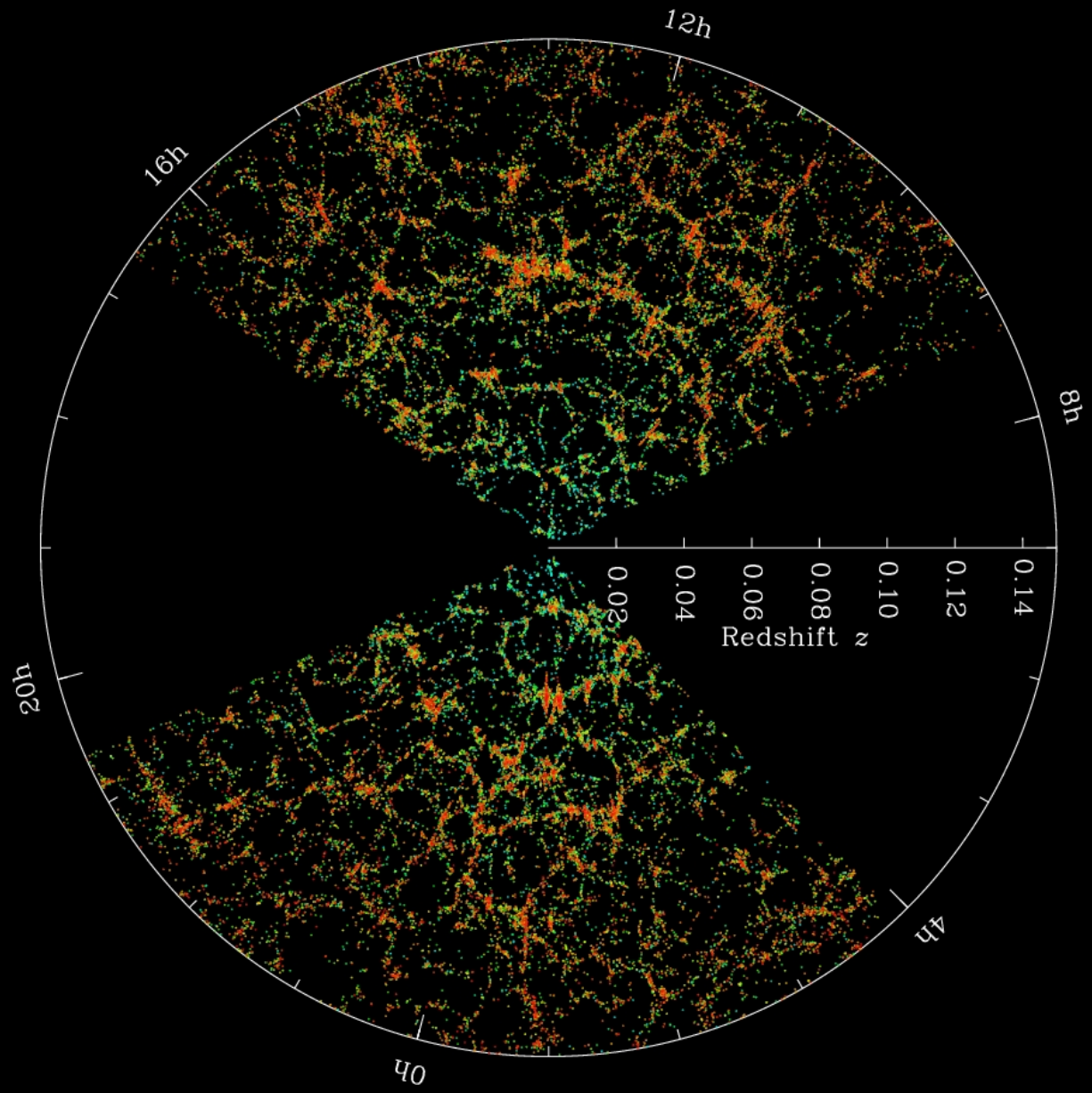
12h
16h
8h
20h
4h
0h
0.02
0.04
0.06
0.08
0.10
0.12
0.14
Redshift z

We have entered an era of concordance cosmology.

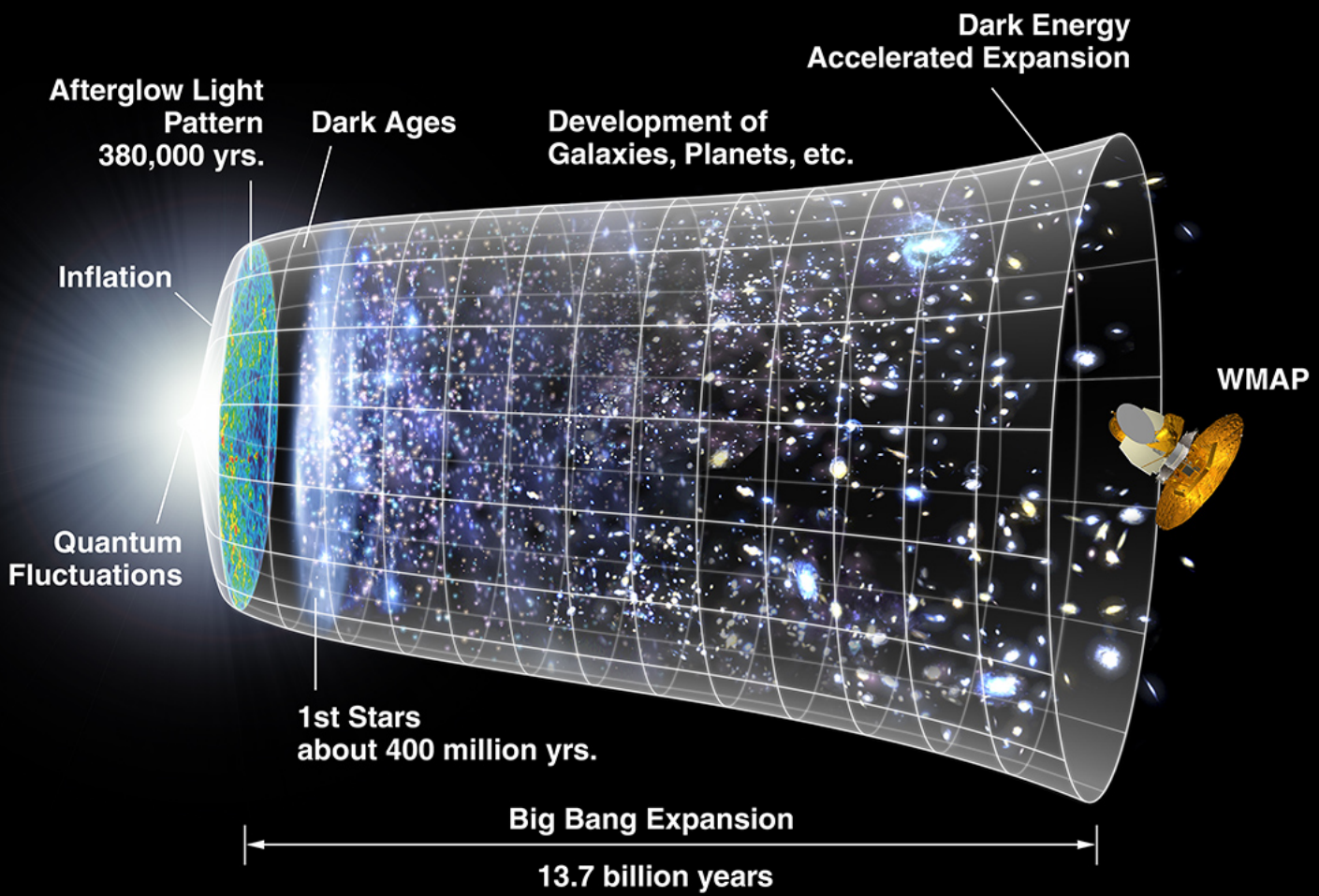

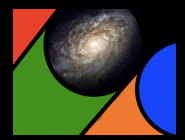

Cosmological observations

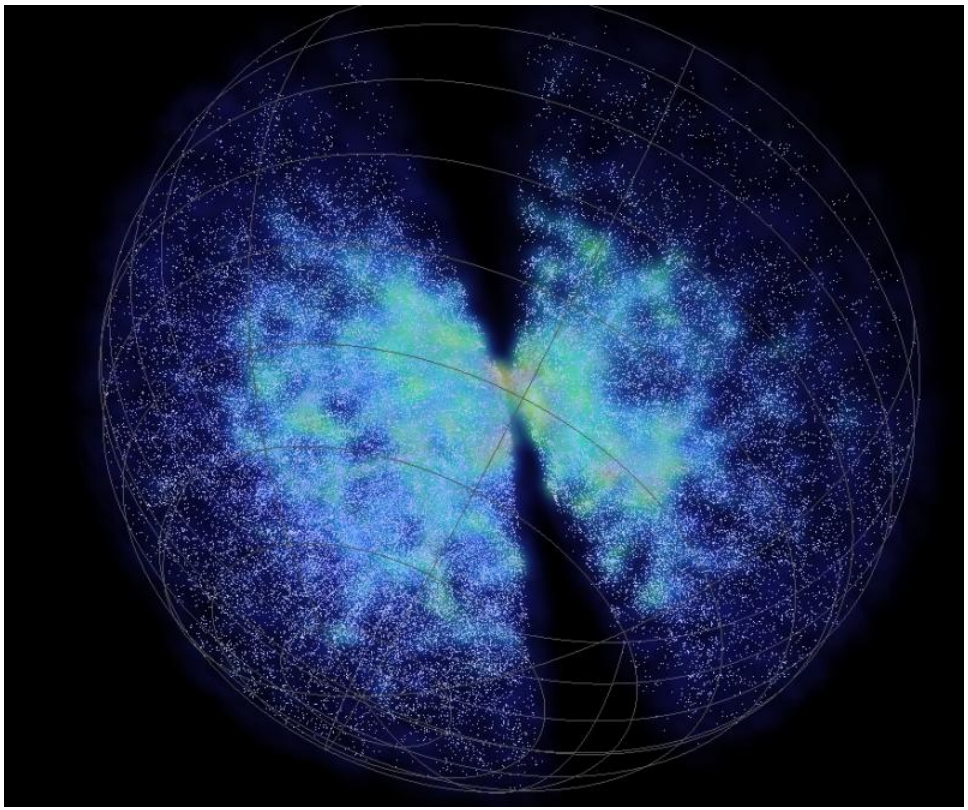

(a) Large-scale structure [Credit: SDSS]

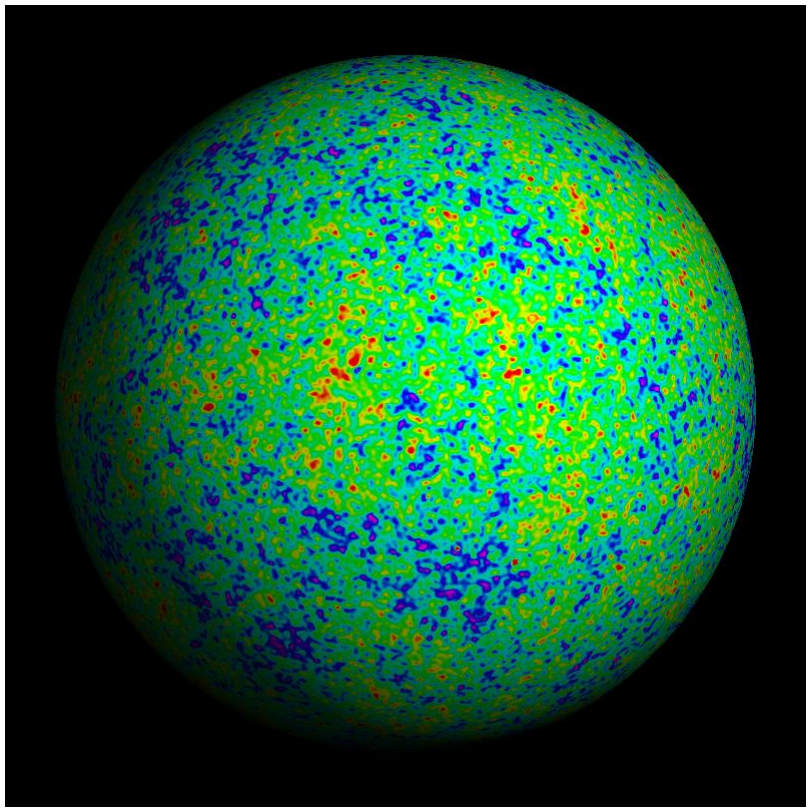

(b) Cosmic microwave background [Credit: WMAP]

Figure: Cosmological observations

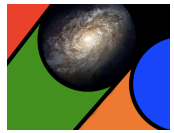

Cosmic microwave background (CMB)

Origin of CMB

1. Temperature of early Universe sufficiently hot that photons had enough energy to ionise hydrogen.
2. Universe opaque photon-baryon fluid.
3. As Universe expanded it cooled, until photons no longer had sufficient energy to ionise hydrogen.
4. Photons decoupled from baryons and the Universe became transparent to radiation.

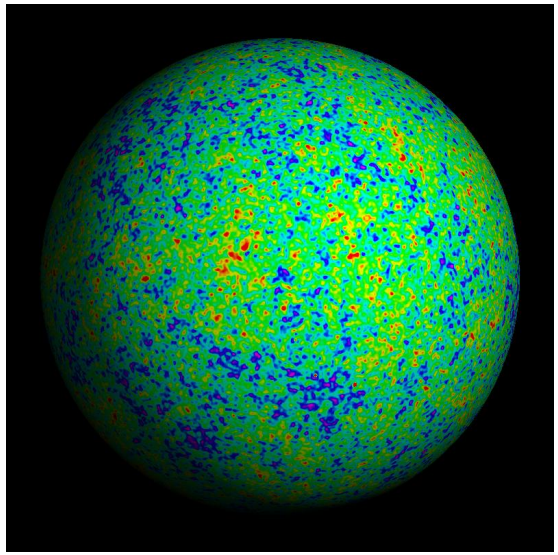

Figure: CMB

- *Recombination* occurred when temperature of Universe dropped to 3000K, about 400,000 years after the Big Bang.
- Photons then free to propagate largely unhindered and observed today on celestial sphere as CMB radiation.
- CMB is highly uniform over the celestial sphere, however it contains small fluctuations at a relative level of 10^{-5} due to acoustic oscillations in the early Universe.

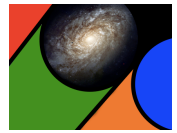

Cosmic microwave background (CMB)

Origin of CMB

1. Temperature of early Universe sufficiently hot that photons had enough energy to ionise hydrogen.
2. Universe opaque photon-baryon fluid.
3. As Universe expanded it cooled, until photons no longer had sufficient energy to ionise hydrogen.
4. Photons decoupled from baryons and the Universe became transparent to radiation.

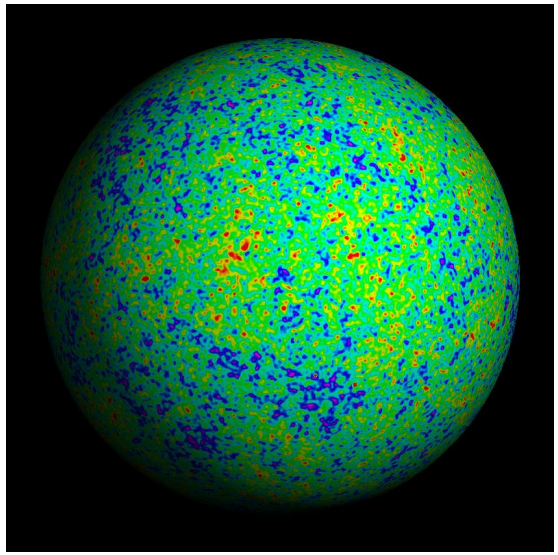

Figure: CMB

- *Recombination* occurred when temperature of Universe dropped to 3000K, about 400,000 years after the Big Bang.
- Photons then free to propagate largely unhindered and observed today on celestial sphere as CMB radiation.
- CMB is highly uniform over the celestial sphere, however it contains small fluctuations at a relative level of 10^{-5} due to acoustic oscillations in the early Universe.

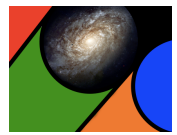

Telescopes and satellites

(a) SDSS (b) DES (c) Euclid

Figure: LSS observations

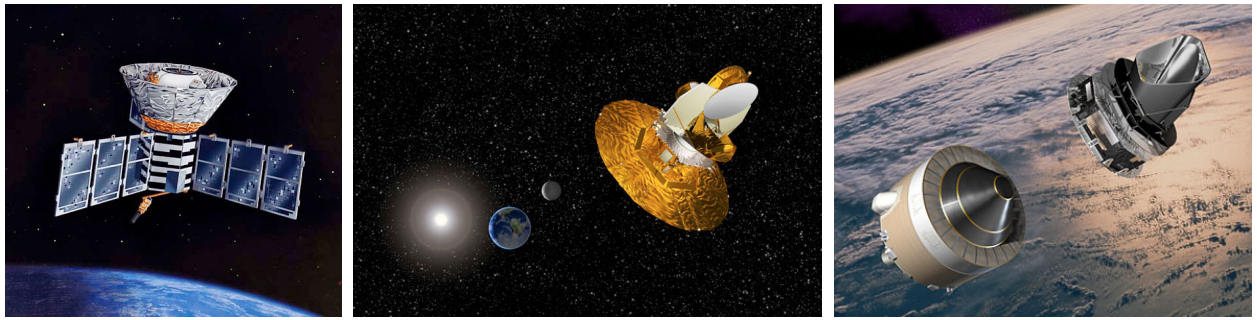

(a) COBE (b) WMAP (c) Planck

Figure: Full-sky CMB observations

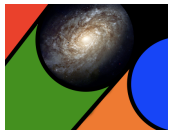

Observations made on the celestial sphere

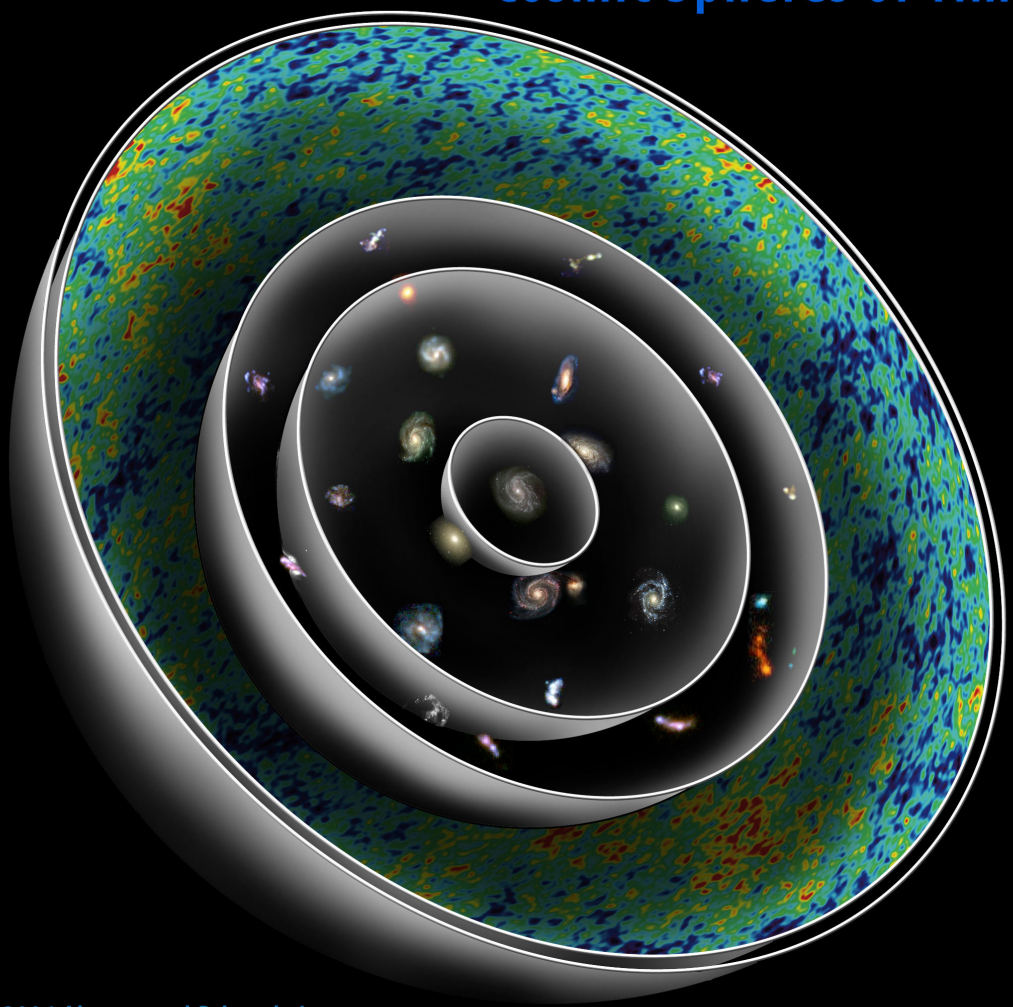

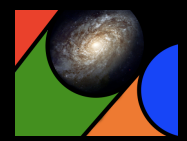

Precision cosmology

Case study: CMB

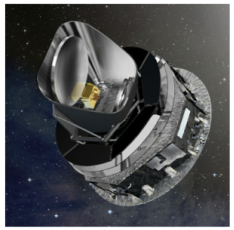

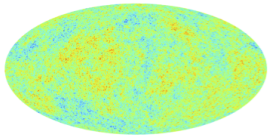

Observation

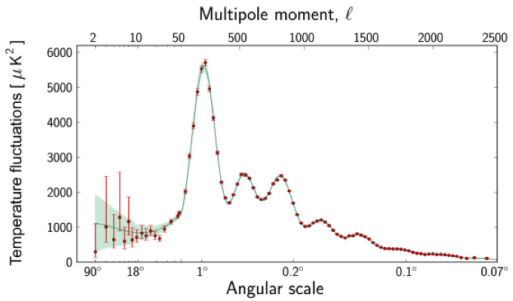

$$P(\Theta|d, M) \propto P(d|\Theta, M)P(\Theta|M)$$

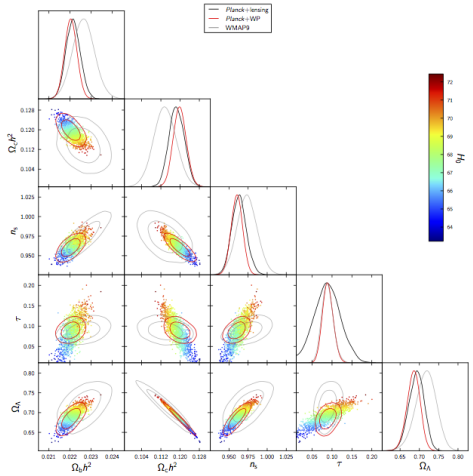

Bayesian Inference

$$\Theta^\star = (A_s^\star, n_s^\star, \tau^\star, \Omega_\mathrm{b}^\star h^2, \Omega_\mathrm{c}^\star h^2, \Omega_\Lambda^\star)$$

$$\Theta = (A_s, n_s, \tau, \Omega_\mathrm{b} h^2, \Omega_\mathrm{c} h^2, \Omega_\Lambda)$$

Theory

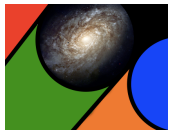

Precision cosmology

Case study: CMB

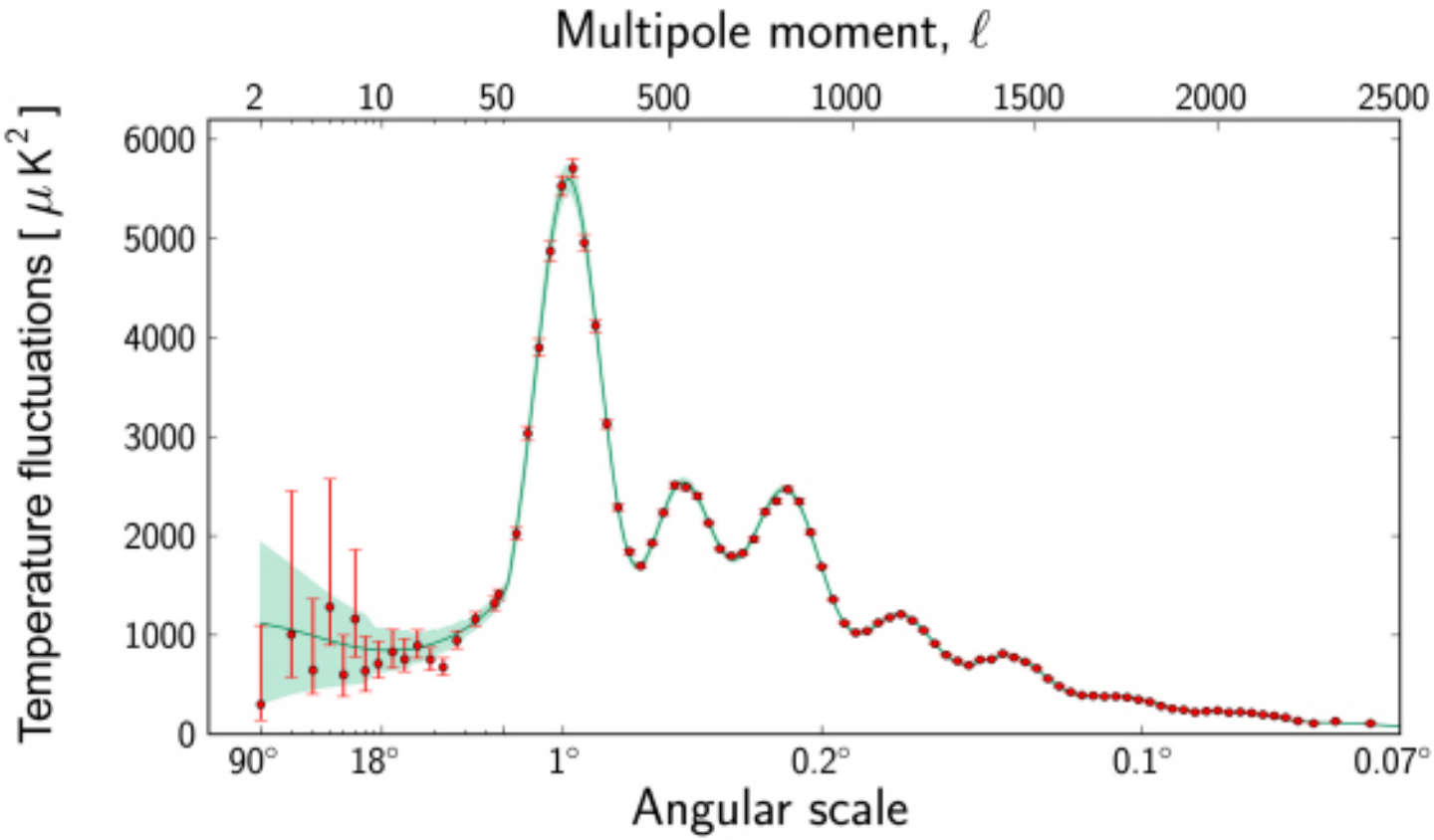

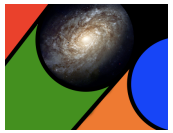

Outstanding questions

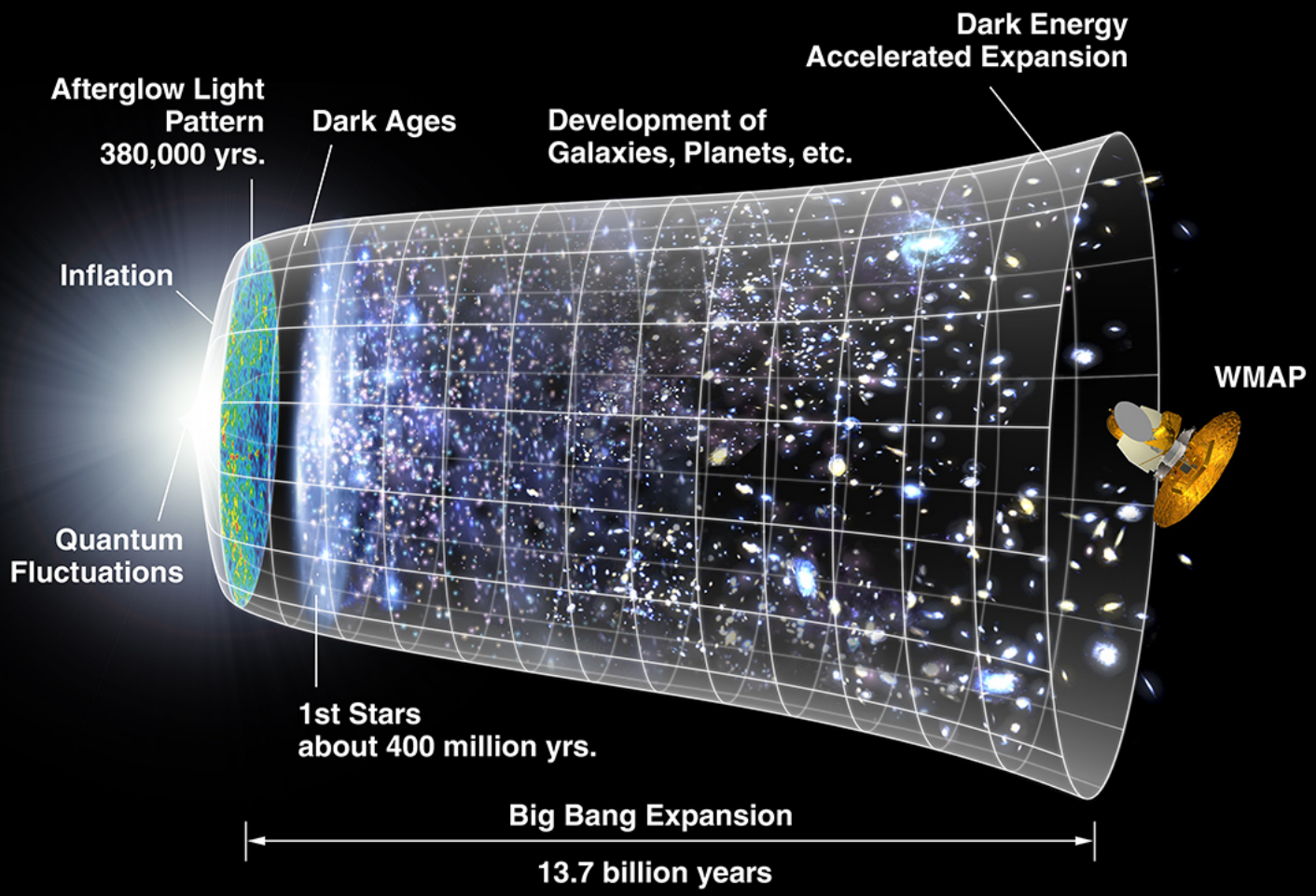

Outline

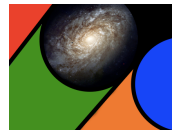

Dark energy

- Universe consists of ordinary baryonic matter, cold dark matter and dark energy.
- Dark energy represents energy density of empty space, which acts as a repulsive force.
- Strong evidence for dark energy exists but we know very little about its nature and origin.
- A consistent model in the framework of particle physics lacking.

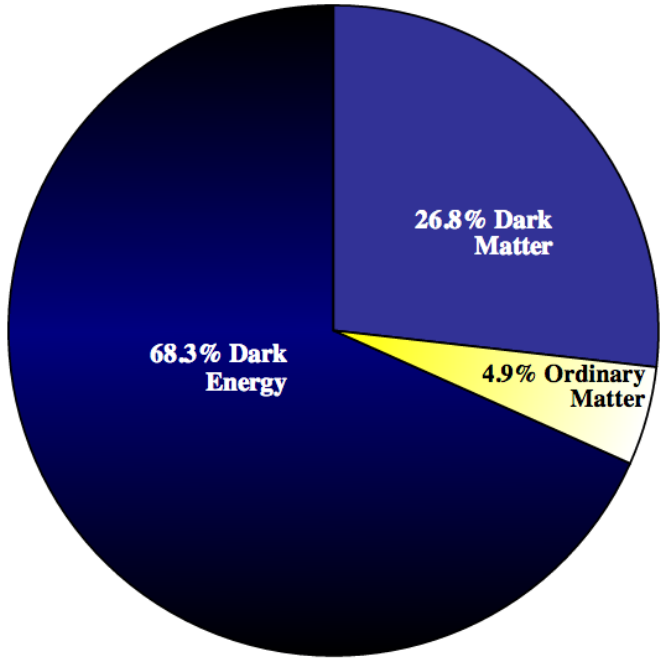

Figure: Content of the Universe [Credit: Planck]

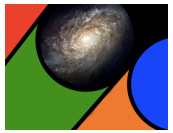

Dark energy

- Universe consists of ordinary baryonic matter, cold dark matter and dark energy.
- Dark energy represents energy density of empty space, which acts as a repulsive force.
- Strong evidence for dark energy exists but we know very little about its nature and origin.
- A consistent model in the framework of particle physics lacking.

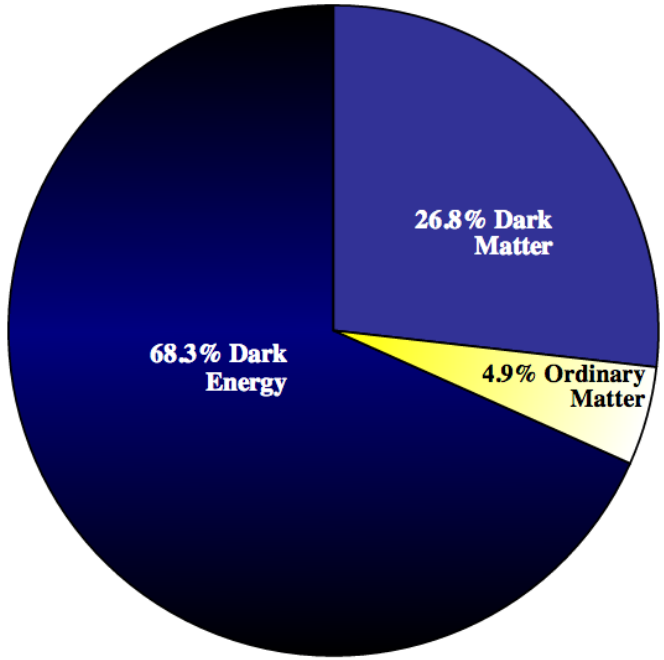

Figure: Content of the Universe [Credit: Planck]

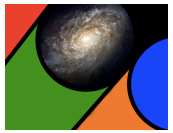

Integrated Sachs Wolfe Effect

Analogy

(no dark energy)

(with dark energy)

(a) No dark energy

(b) With dark energy

Figure: Analogy of ISW effect

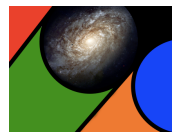

Integrated Sachs Wolfe Effect

Correlation between CMB and LSS

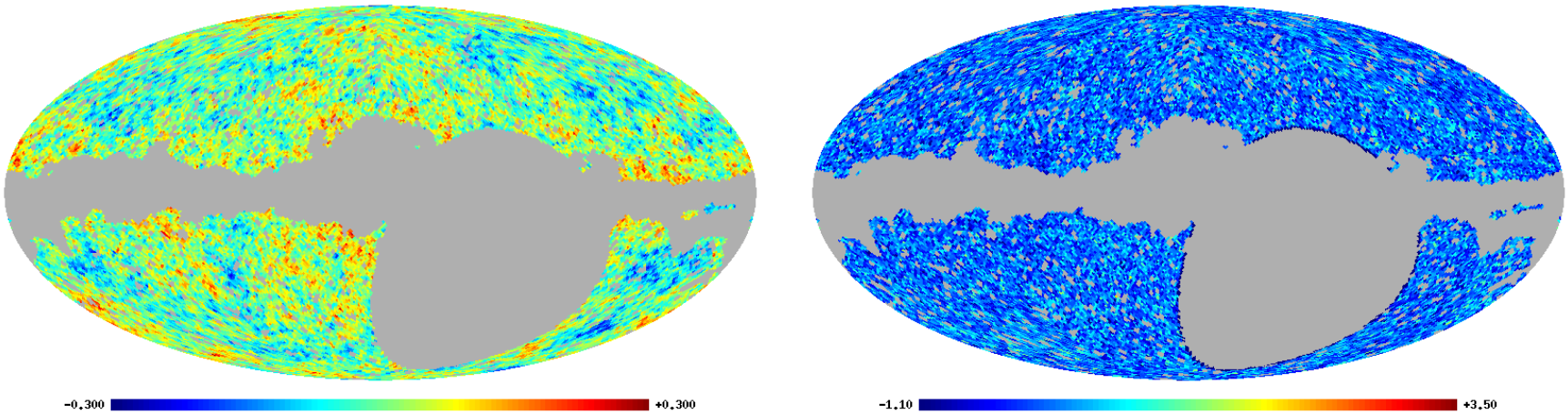

(a) CMB (b) LSS

Figure: Constraining dark energy through any correlation between the CMB and LSS.

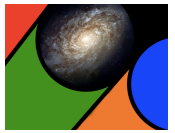

Recall wavelet transform in Euclidean space

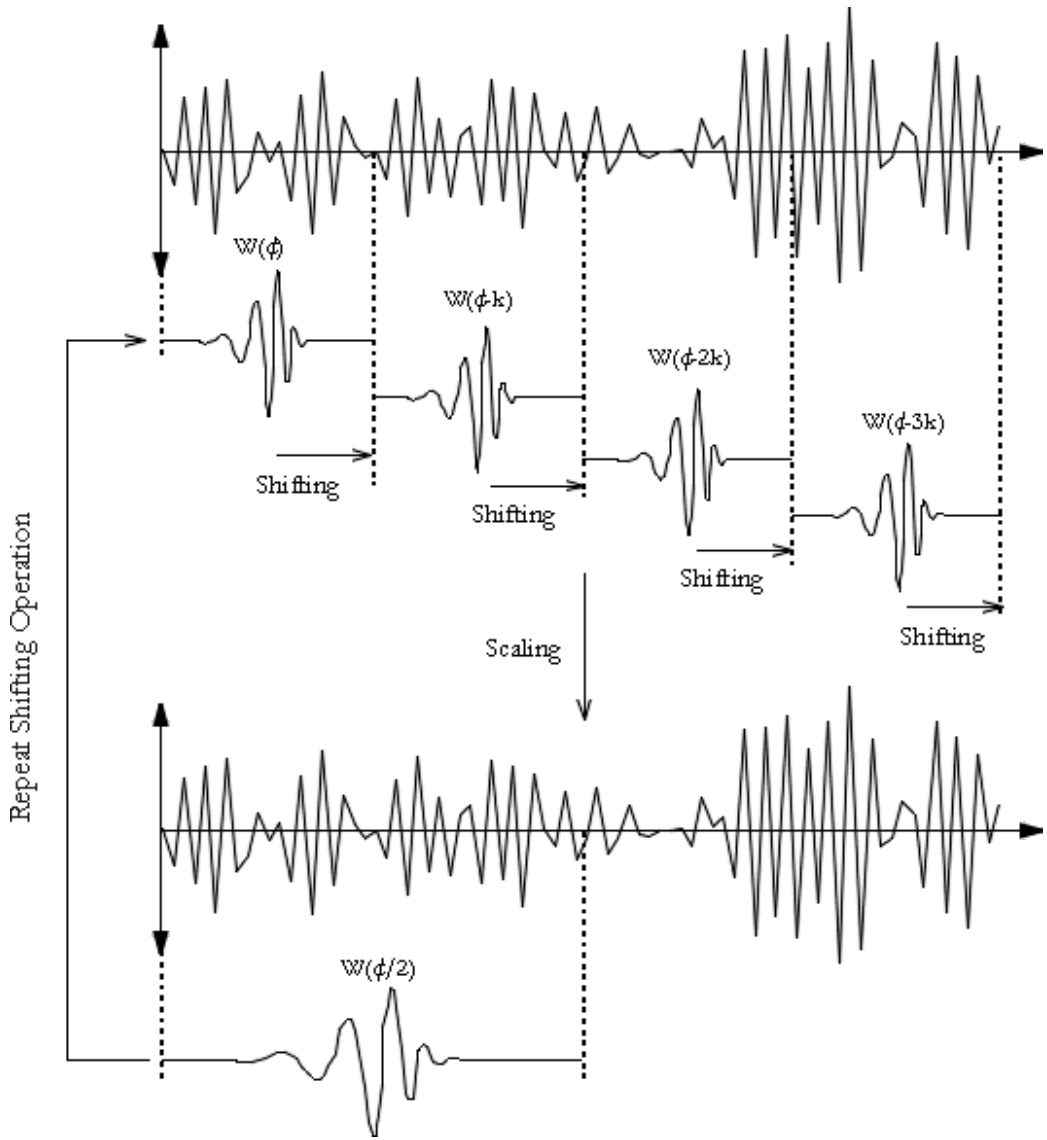

Figure: Wavelet scaling and shifting [Credit: http://www.wavelet.org/tutorial/]

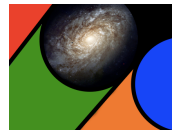

Continuous wavelets on the sphere

- One of the first natural wavelet construction on the sphere was derived in the seminal work of Antoine and Vandergheynst (1998) (reintroduced by Wiaux 2005).
- Construct wavelet atoms from affine transformations (dilation, translation) on the sphere of a mother wavelet.
- The natural extension of translations to the sphere are rotations. Rotation of a function f on the sphere is defined by

$$[\mathcal{R}(\rho)f](\omega) = f(\rho^{-1}\cdot\omega), \quad \omega = (\theta,\varphi)\in\mathbb{S}^2, \quad \rho = (\alpha,\beta,\gamma)\in \mathrm{SO}(3)\ .$$

translation

- How define dilation on the sphere?
- The spherical dilation operator is defined through the conjugation of the Euclidean dilation and stereographic projection Π:

$$\mathcal{D}(a) \equiv \Pi^{-1}\, d(a)\, \Pi\ .$$

dilation

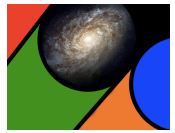

Continuous wavelets on the sphere

- One of the first natural wavelet construction on the sphere was derived in the seminal work of Antoine and Vandergheynst (1998) (reintroduced by Wiaux 2005).
- Construct wavelet atoms from affine transformations (dilation, translation) on the sphere of a mother wavelet.
- The natural extension of translations to the sphere are rotations. Rotation of a function f on the sphere is defined by

$$[\mathcal{R}(\rho)f](\omega) = f(\rho^{-1} \cdot \omega), \quad \omega = (\theta, \varphi) \in \mathbb{S}^2, \quad \rho = (\alpha, \beta, \gamma) \in \mathrm{SO}(3) \; .$$

translation

- How define dilation on the sphere?
- The spherical dilation operator is defined through the conjugation of the Euclidean dilation and stereographic projection Π:

$$\mathcal{D}(a) \equiv \Pi^{-1} \, d(a) \, \Pi \; .$$

dilation

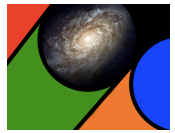

Continuous wavelets on the sphere

- One of the first natural wavelet construction on the sphere was derived in the seminal work of Antoine and Vandergheynst (1998) (reintroduced by Wiaux 2005).
- Construct wavelet atoms from affine transformations (dilation, translation) on the sphere of a mother wavelet.
- The natural extension of translations to the sphere are rotations. Rotation of a function f on the sphere is defined by

$$[\mathcal{R}(\rho)f](\omega) = f(\rho^{-1} \cdot \omega), \quad \omega = (\theta, \varphi) \in \mathbb{S}^2, \quad \rho = (\alpha, \beta, \gamma) \in \mathrm{SO}(3) \, .$$

translation

- How define dilation on the sphere?
- The spherical dilation operator is defined through the conjugation of the Euclidean dilation and stereographic projection Π:

$$\mathcal{D}(a) \equiv \Pi^{-1} \, d(a) \, \Pi \, .$$

dilation

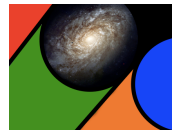

Continuous wavelets on the sphere

- One of the first natural wavelet construction on the sphere was derived in the seminal work of Antoine and Vandergheynst (1998) (reintroduced by Wiaux 2005).
- Construct wavelet atoms from affine transformations (dilation, translation) on the sphere of a mother wavelet.
- The natural extension of translations to the sphere are rotations. Rotation of a function f on the sphere is defined by

$$[\mathcal{R}(\rho)f](\omega) = f(\rho^{-1}\cdot\omega), \quad \omega = (\theta,\varphi)\in\mathbb{S}^2, \quad \rho = (\alpha,\beta,\gamma)\in \mathrm{SO}(3)\,.$$

translation

- How define dilation on the sphere?
- The spherical dilation operator is defined through the conjugation of the Euclidean dilation and stereographic projection Π:

$$\mathcal{D}(a) \equiv \Pi^{-1}\, d(a)\, \Pi\,.$$

dilation

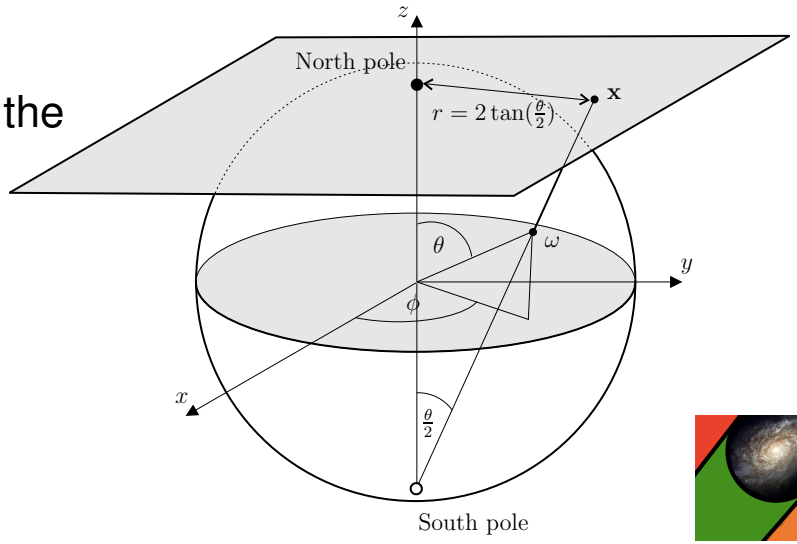

Continuous wavelets on the sphere

Forward transform (*i.e.* analysis)

- Wavelet family on the sphere constructed from rotations and dilations of a mother wavelet Ψ:

$$\{\Psi_{a,\rho} \equiv \mathcal{R}(\rho)\mathcal{D}(a)\Psi : \rho \in \mathrm{SO}(3), a \in \mathbb{R}^+_*\} \,.$$

dictionary

- The forward wavelet transform is given by

$$W^f_\Psi(a,\rho) = \langle f, \Psi_{a,\rho}\rangle \equiv \int_{\mathbb{S}^2} \mathrm{d}\Omega(\omega)\, f(\omega)\, \Psi^*_{a,\rho}(\omega) \,,$$

projection

where $\mathrm{d}\Omega(\omega) = \sin\theta\, \mathrm{d}\theta\, \mathrm{d}\varphi$ is the usual invariant measure on the sphere.

- Wavelet coefficients live in $\mathrm{SO}(3) \times \mathbb{R}^+_*$; thus, directional structure is naturally incorporated.

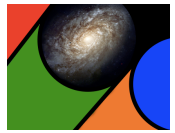

Continuous wavelets on the sphere

Forward transform (*i.e.* analysis)

- Wavelet family on the sphere constructed from rotations and dilations of a mother wavelet Ψ:

$$\{\Psi_{a,\rho} \equiv \mathcal{R}(\rho)\mathcal{D}(a)\Psi : \rho \in \mathrm{SO}(3), a \in \mathbb{R}^+_*\} \,.$$

dictionary

- The forward wavelet transform is given by

$$W^f_\Psi(a,\rho) = \langle f, \Psi_{a,\rho}\rangle \equiv \int_{\mathbb{S}^2} \mathrm{d}\Omega(\omega)\, f(\omega)\, \Psi^*_{a,\rho}(\omega) \,,$$

projection

where $\mathrm{d}\Omega(\omega) = \sin\theta\, \mathrm{d}\theta\, \mathrm{d}\varphi$ is the usual invariant measure on the sphere.

- Wavelet coefficients live in $\mathrm{SO}(3) \times \mathbb{R}^+_*$; thus, directional structure is naturally incorporated.

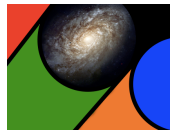

Continuous wavelets on the sphere

Forward transform (*i.e.* analysis)

- Wavelet family on the sphere constructed from rotations and dilations of a mother wavelet Ψ:

$$\{\Psi_{a,\rho} \equiv \mathcal{R}(\rho)\mathcal{D}(a)\Psi : \rho \in \mathrm{SO}(3), a \in \mathbb{R}^+_*\} \,.$$

dictionary

- The forward wavelet transform is given by

$$W^f_\Psi(a,\rho) = \langle f, \Psi_{a,\rho}\rangle \equiv \int_{\mathbb{S}^2} \mathrm{d}\Omega(\omega)\, f(\omega)\, \Psi^*_{a,\rho}(\omega) \,,$$

projection

where $\mathrm{d}\Omega(\omega) = \sin\theta\, \mathrm{d}\theta\, \mathrm{d}\varphi$ is the usual invariant measure on the sphere.

- Wavelet coefficients live in $\mathrm{SO}(3) \times \mathbb{R}^+_*$; thus, directional structure is naturally incorporated.

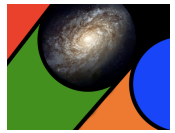

Continuous wavelets on the sphere

Fast algorithms

- Fast algorithms essential (for a review see Wiaux, McEwen & Vielva 2007)
  - Factoring of rotations: McEwen *et al.* (2007), Wandelt & Gorski (2001), Risbo (1996)
  - Separation of variables: Wiaux *et al.* (2005)

FastCSWT code `http://www.fastcswt.org`

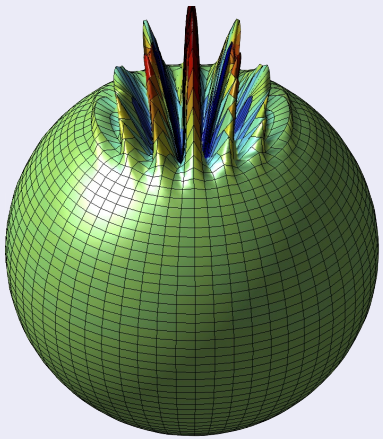

Fast directional continuous spherical wavelet transform algorithms
McEwen *et al.* (2007)

- Fortran
- Supports directional and steerable wavelets

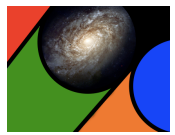

Continuous wavelets on the sphere

Mother wavelets

- Correspondence principle between spherical and Euclidean wavelets (Wiaux *et al.* 2005).
- Mother wavelets on sphere constructed from the projection of mother Euclidean wavelets defined on the plane:

$$\Psi = \Pi^{-1} \Psi_{\mathbb{R}^2},$$

construction

where $\Psi_{\mathbb{R}^2} \in \mathrm{L}^2(\mathbb{R}^2, \mathrm{d}^2\boldsymbol{x})$ is an admissible wavelet on the plane.

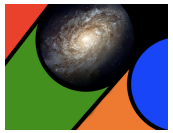

Continuous wavelets on the sphere

Mother wavelets

- Correspondence principle between spherical and Euclidean wavelets (Wiaux *et al.* 2005).
- Mother wavelets on sphere constructed from the projection of mother Euclidean wavelets defined on the plane:

$$\boxed{\Psi = \Pi^{-1} \Psi_{\mathbb{R}^2}}, \quad \text{construction}$$

where $\Psi_{\mathbb{R}^2} \in \mathrm{L}^2(\mathbb{R}^2, \mathrm{d}^2\boldsymbol{x})$ is an admissible wavelet on the plane.

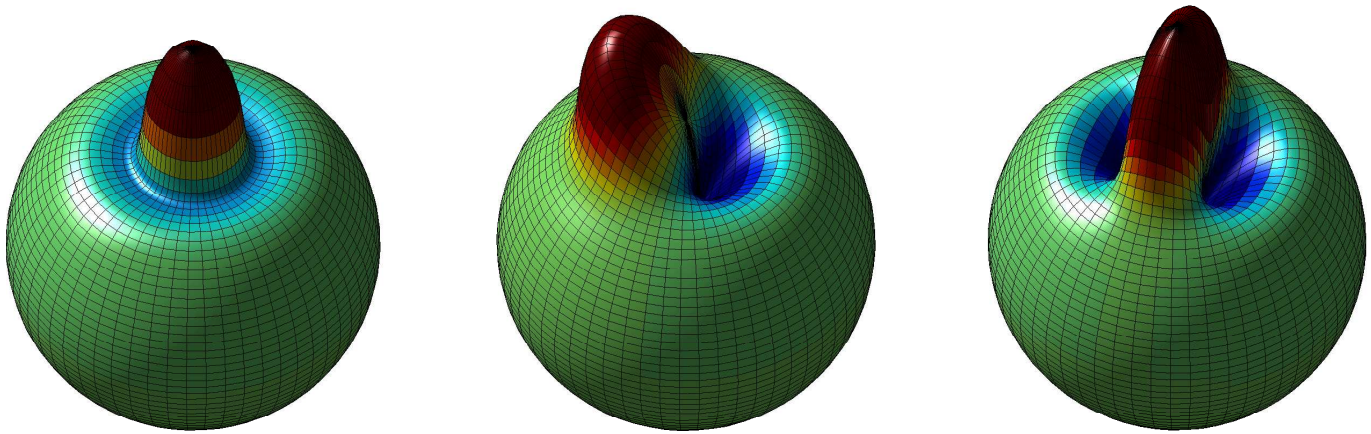

(a) SMHW (b) SBW (c) S2GDW

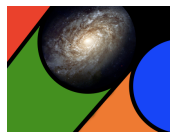

Figure: Spherical wavelets at scale $a, b = 0.2$.

Continuous wavelets on the sphere

Inverse transform (*i.e.* synthesis)

- The inverse wavelet transform given by

$$f(\omega) = \underbrace{\int_0^\infty \frac{\mathrm{d}a}{a^3} \int_{\mathrm{SO}(3)} \mathrm{d}\varrho(\rho)}_{\text{'sum' contributions}} \underbrace{W_\Psi^f(a,\rho)\, [\mathcal{R}(\rho)\widehat{L}_\Psi \Psi_a](\omega)}_{\text{weighted basis functions}},$$

  where $\mathrm{d}\varrho(\rho) = \sin\beta\, \mathrm{d}\alpha\, \mathrm{d}\beta\, \mathrm{d}\gamma$ is the invariant measure on the rotation group $\mathrm{SO}(3)$.

- Perfect reconstruction iff wavelets satisfy admissibility property:

$$0 < \widehat{C}_\Psi^\ell \equiv \frac{8\pi^2}{2\ell+1} \sum_{m=-\ell}^{\ell} \int_0^\infty \frac{\mathrm{d}a}{a^3} \mid (\Psi_a)_{\ell m} \mid^2 < \infty, \quad \forall \ell \in \mathbb{N}$$

  where $(\Psi_a)_{\ell m}$ are the spherical harmonic coefficients of $\Psi_a(\omega)$.

- BUT... exact reconstruction not feasible in practice!

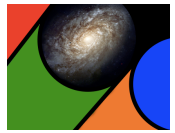

Continuous wavelets on the sphere

Inverse transform (*i.e.* synthesis)

- The inverse wavelet transform given by

$$f(\omega) = \underbrace{\int_0^\infty \frac{\mathrm{d}a}{a^3} \int_{\mathrm{SO}(3)} \mathrm{d}\varrho(\rho)}_{\text{'sum' contributions}} \underbrace{W_\Psi^f(a,\rho)\, [\mathcal{R}(\rho)\widehat{L}_\Psi \Psi_a](\omega)}_{\text{weighted basis functions}},$$

  where $\mathrm{d}\varrho(\rho) = \sin\beta\, \mathrm{d}\alpha\, \mathrm{d}\beta\, \mathrm{d}\gamma$ is the invariant measure on the rotation group $\mathrm{SO}(3)$.

- Perfect reconstruction iff wavelets satisfy admissibility property:

$$0 < \widehat{C}_\Psi^\ell \equiv \frac{8\pi^2}{2\ell+1} \sum_{m=-\ell}^{\ell} \int_0^\infty \frac{\mathrm{d}a}{a^3} \mid (\Psi_a)_{\ell m} \mid^2 < \infty, \quad \forall \ell \in \mathbb{N}$$

  where $(\Psi_a)_{\ell m}$ are the spherical harmonic coefficients of $\Psi_a(\omega)$.

- BUT... exact reconstruction not feasible in practice!

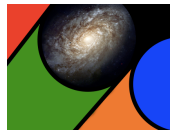

Continuous wavelets on the sphere

Inverse transform (*i.e.* synthesis)

- The inverse wavelet transform given by

$$f(\omega) = \underbrace{\int_0^\infty \frac{\mathrm{d}a}{a^3} \int_{\mathrm{SO}(3)} \mathrm{d}\varrho(\rho)}_{\text{'sum' contributions}} \underbrace{W_\Psi^f(a,\rho)\, [\mathcal{R}(\rho)\widehat{L}_\Psi \Psi_a](\omega)}_{\text{weighted basis functions}},$$

  where $\mathrm{d}\varrho(\rho) = \sin\beta\, \mathrm{d}\alpha\, \mathrm{d}\beta\, \mathrm{d}\gamma$ is the invariant measure on the rotation group $\mathrm{SO}(3)$.

- Perfect reconstruction iff wavelets satisfy admissibility property:

$$0 < \widehat{C}_\Psi^\ell \equiv \frac{8\pi^2}{2\ell+1} \sum_{m=-\ell}^{\ell} \int_0^\infty \frac{\mathrm{d}a}{a^3} \mid (\Psi_a)_{\ell m} \mid^2 < \infty, \quad \forall \ell \in \mathbb{N}$$

  where $(\Psi_a)_{\ell m}$ are the spherical harmonic coefficients of $\Psi_a(\omega)$.

- BUT... exact reconstruction not feasible in practice!

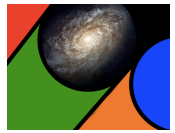

Detecting dark energy

Wavelet coefficient correlation

- Compute wavelet correlation of CMB and LSS data (McEwen *et al.* 2007, McEwen *et al.* 2008).
- Compare to 1000 Monte Carlo simulations.
- Correlation detected at 99.9% significance.

$\Rightarrow$ Independent evidence for the existence of dark energy!

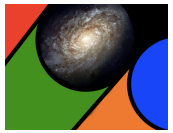

Detecting dark energy

Wavelet coefficient correlation

- Compute wavelet correlation of CMB and LSS data (McEwen *et al.* 2007, McEwen *et al.* 2008).
- Compare to 1000 Monte Carlo simulations.
- Correlation detected at 99.9% significance.

$\Rightarrow$ Independent evidence for the existence of dark energy!

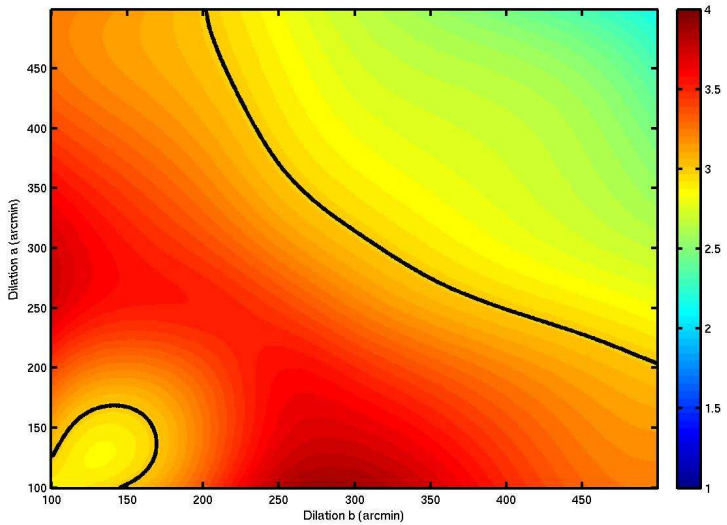

Figure: Wavelet correlation N_σ surface. Contours are shown at 3σ.

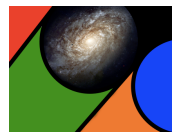

Detecting dark energy

Constraining cosmological models

- Use positive detection of the ISW effect to constrain parameters of cosmological models:
  - Energy density Ω_Λ.
  - Equation of state parameter w relating pressure and density of cosmological fluid modelling dark energy, *i.e.* $p = w\rho$.
- Parameter estimates of $\Omega_\Lambda = 0.63^{+0.18}_{-0.17}$ and $w = -0.77^{+0.35}_{-0.36}$ obtained.

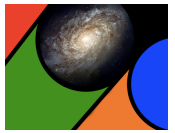

Detecting dark energy

Constraining cosmological models

- Use positive detection of the ISW effect to constrain parameters of cosmological models:
  - Energy density Ω_Λ.
  - Equation of state parameter w relating pressure and density of cosmological fluid modelling dark energy, *i.e.* $p = w\rho$.
- Parameter estimates of $\Omega_\Lambda = 0.63^{+0.18}_{-0.17}$ and $w = -0.77^{+0.35}_{-0.36}$ obtained.

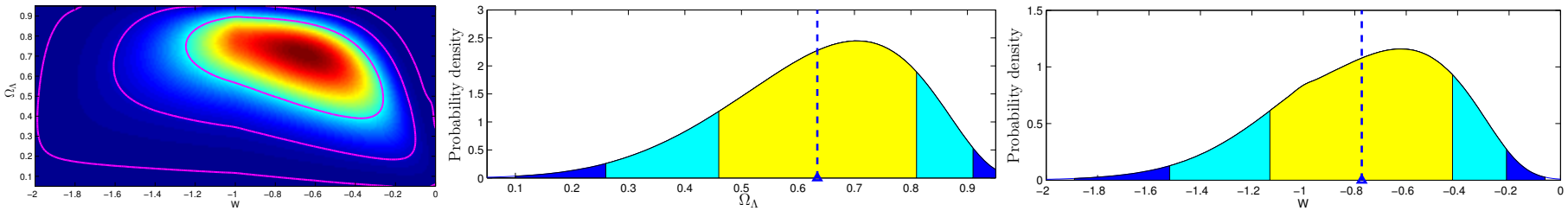

(a) Full likelihood surface (b) Marginalised distribution for Ω_Λ (c) Marginalised distribution for w

Figure: Likelihood for dark energy parameters.

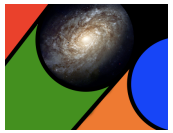

Outline

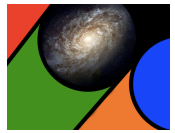

Cosmic strings

- Symmetry breaking phase transitions in the early Universe $\rightarrow$ topological defects.
- Cosmic strings well-motivated phenomenon that arise when axial or cylindrical symmetry is broken $\rightarrow$ line-like discontinuities in the fabric of the Universe.
- We have not yet observed cosmic strings but we have observed string-like topological defects in other media.

The detection of cosmic strings would open a new window into the physics of the Universe!

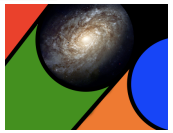

Cosmic strings

- Symmetry breaking phase transitions in the early Universe $\rightarrow$ topological defects.
- Cosmic strings well-motivated phenomenon that arise when axial or cylindrical symmetry is broken $\rightarrow$ line-like discontinuities in the fabric of the Universe.
- We have not yet observed cosmic strings but we have observed string-like topological defects in other media.

Figure: Optical microscope photograph of a thin film of freely suspended nematic liquid crystal after a temperature quench.
[Credit: Chuang *et al.* (1991).]

The detection of cosmic strings would open a new window into the physics of the Universe!

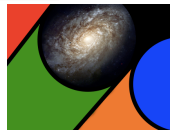

Cosmic strings

- Symmetry breaking phase transitions in the early Universe $\rightarrow$ topological defects.
- Cosmic strings well-motivated phenomenon that arise when axial or cylindrical symmetry is broken $\rightarrow$ line-like discontinuities in the fabric of the Universe.
- We have not yet observed cosmic strings but we have observed string-like topological defects in other media.

Figure: Optical microscope photograph of a thin film of freely suspended nematic liquid crystal after a temperature quench.
[Credit: Chuang *et al.* (1991).]

The detection of cosmic strings would open a new window into the physics of the Universe!

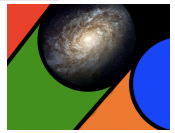

Observational signatures of cosmic strings

Conical Spacetime

- Spacetime about a cosmic string is conical, with a three-dimensional wedge removed (Vilenkin 1981).
- Strings moving transverse to the line of sight induce line-like discontinuities in the CMB (Kaiser & Stebbins 1984).
- The amplitude of the induced contribution scales with the string tension $G\mu$.

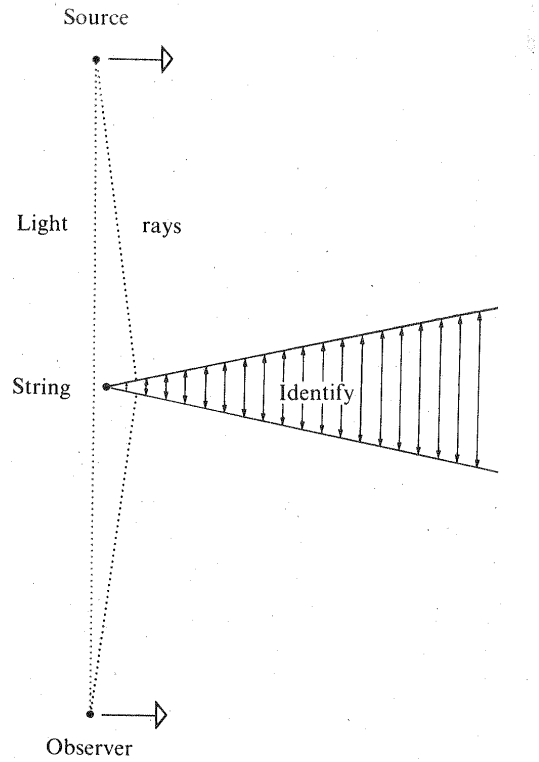

Figure: Spacetime around a cosmic string.
[Credit: Kaiser & Stebbins 1984, DAMTP.]

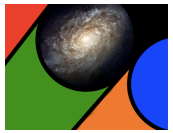

Observational signatures of cosmic strings

CMB contribution

- Make contact between theory and data using high-resolution simulations.
- Search for a weak string signal s embedded in the CMB c, with observations d given by

$$\underbrace{d(\theta,\varphi)}_{\text{observation}} = \underbrace{c(\theta,\varphi)}_{\text{CMB}} + \underbrace{G\mu \cdot s(\theta,\varphi)}_{\text{strings}} .$$

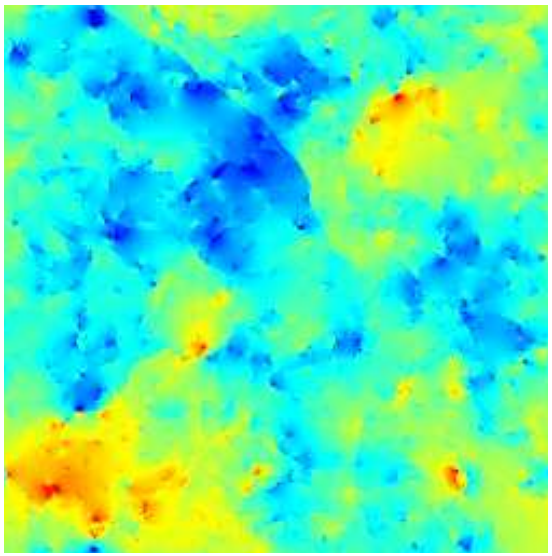

(a) Flat patch (Fraisse *et al.* 2008)

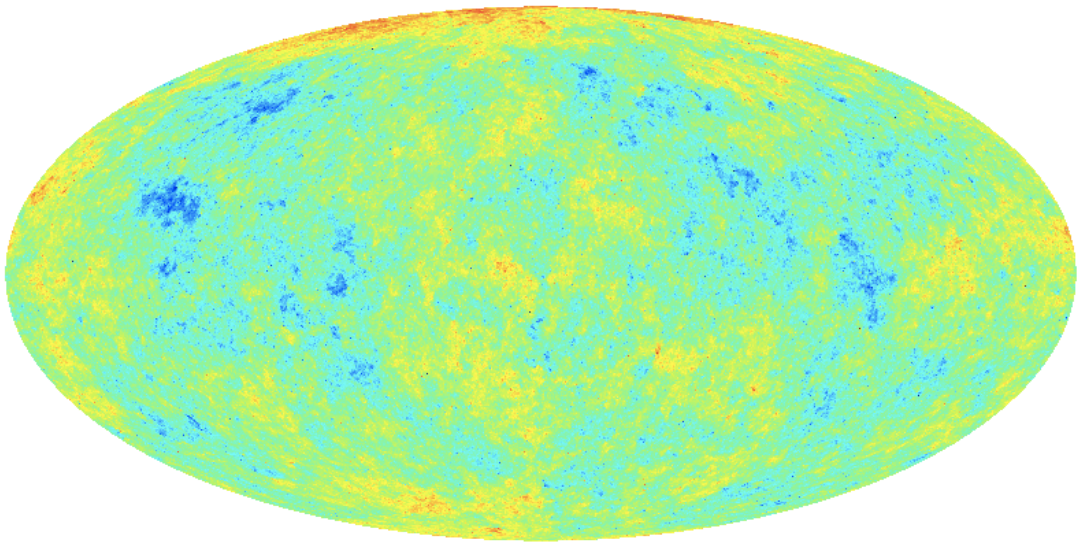

(b) Full-sky (Ringeval *et al.* 2012)

Figure: Cosmic string simulations.

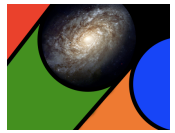

Observational signatures of cosmic strings

CMB contribution

- Make contact between theory and data using high-resolution simulations.
- Search for a weak string signal s embedded in the CMB c, with observations d given by

$$\underbrace{d(\theta,\varphi)}_{\text{observation}} = \underbrace{c(\theta,\varphi)}_{\text{CMB}} + \underbrace{G\mu \cdot s(\theta,\varphi)}_{\text{strings}}.$$

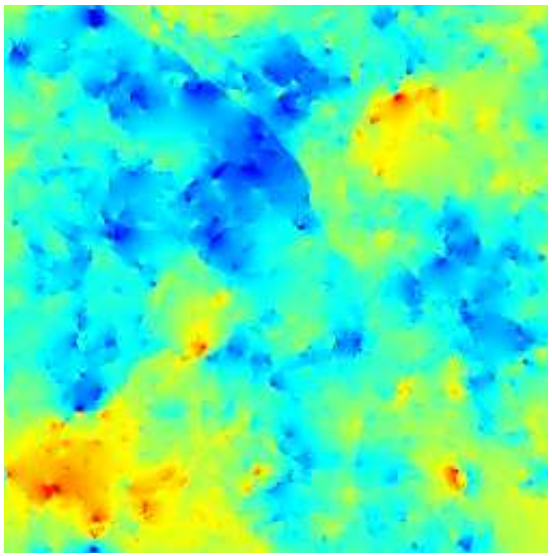

(a) Flat patch (Fraisse *et al.* 2008)

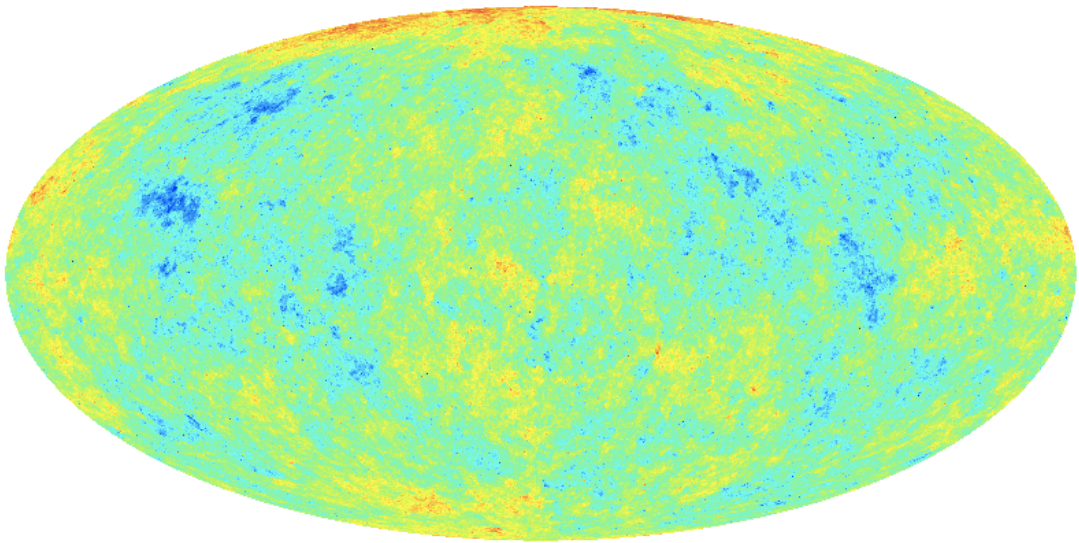

(b) Full-sky (Ringeval *et al.* 2012)

Figure: Cosmic string simulations.

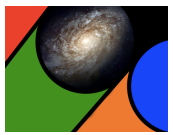

Scale-discretised wavelets on the sphere

Wavelet construction

Exact reconstruction not feasible in practice with continuous wavelets!

- *Exact reconstruction with directional wavelets on the sphere*
  Wiaux, McEwen, Vandergheynst, Blanc (2008)
- Dilation performed in harmonic space [*cf.* McEwen *et al.* (2006), Sanz *et al.* (2006)].
- Scale-discretised wavelet $\Psi^j \in \mathrm{L}^2(\mathbb{S}^2, \mathrm{d}\Omega)$ defined in harmonic space:

$$\Psi^j_{\ell m} \equiv \kappa^j(\ell) s_{\ell m} \, .$$

- Admissible wavelets constructed to satisfy a resolution of the identity:

$$\underbrace{|\Phi_{\ell 0}|^2}_{\text{scaling function}} + \sum_{j=0}^{J} \sum_{m=-\ell}^{\ell} \underbrace{|\Psi^j_{\ell m}|^2}_{\text{wavelet}} = 1 \, , \quad \forall \ell \, .$$

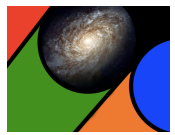

Scale-discretised wavelets on the sphere

Wavelet construction

Exact reconstruction not feasible in practice with continuous wavelets!

- *Exact reconstruction with directional wavelets on the sphere*
  Wiaux, McEwen, Vandergheynst, Blanc (2008)
- Dilation performed in harmonic space [*cf.* McEwen *et al.* (2006), Sanz *et al.* (2006)].
- Scale-discretised wavelet $\Psi^j \in \mathrm{L}^2(\mathbb{S}^2, \mathrm{d}\Omega)$ defined in harmonic space:

$$\Psi^j_{\ell m} \equiv \kappa^j(\ell) s_{\ell m} \, .$$

- Admissible wavelets constructed to satisfy a resolution of the identity:

$$\underbrace{|\Phi_{\ell 0}|^2}_{\text{scaling function}} + \sum_{j=0}^{J} \sum_{m=-\ell}^{\ell} \underbrace{|\Psi^j_{\ell m}|^2}_{\text{wavelet}} = 1 \, , \quad \forall \ell \, .$$

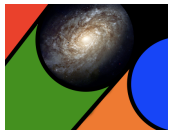

Scale-discretised wavelets on the sphere

Wavelet construction

Exact reconstruction not feasible in practice with continuous wavelets!

- *Exact reconstruction with directional wavelets on the sphere*
  Wiaux, McEwen, Vandergheynst, Blanc (2008)
- Dilation performed in harmonic space [*cf.* McEwen *et al.* (2006), Sanz *et al.* (2006)].

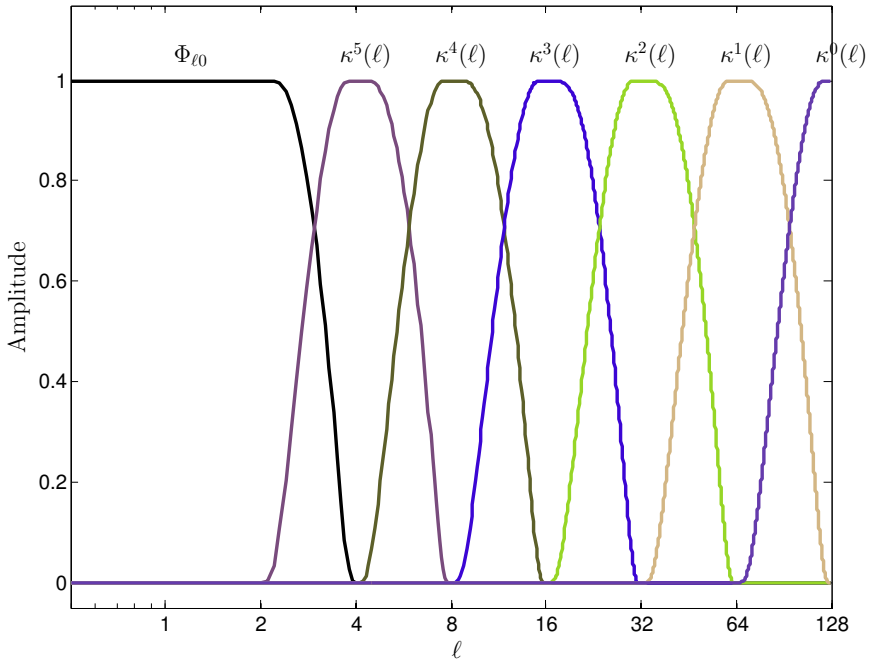

- Scale-discretised wavelet $\Psi^j \in \mathrm{L}^2(\mathbb{S}^2, \mathrm{d}\Omega)$ defined in harmonic space:

$$\Psi^j_{\ell m} \equiv \kappa^j(\ell) s_{\ell m} \, .$$

- Admissible wavelets constructed to satisfy a resolution of the identity:

$$\underbrace{|\Phi_{\ell 0}|^2}_{\text{scaling function}} + \sum_{j=0}^{J} \sum_{m=-\ell}^{\ell} \underbrace{|\Psi^j_{\ell m}|^2}_{\text{wavelet}} = 1 \, , \quad \forall \ell \, .$$

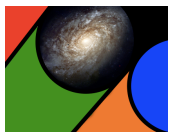

Scale-discretised wavelets on the sphere

Wavelet construction

Exact reconstruction not feasible in practice with continuous wavelets!

- *Exact reconstruction with directional wavelets on the sphere*
  Wiaux, McEwen, Vandergheynst, Blanc (2008)
- Dilation performed in harmonic space [*cf.* McEwen *et al.* (2006), Sanz *et al.* (2006)].

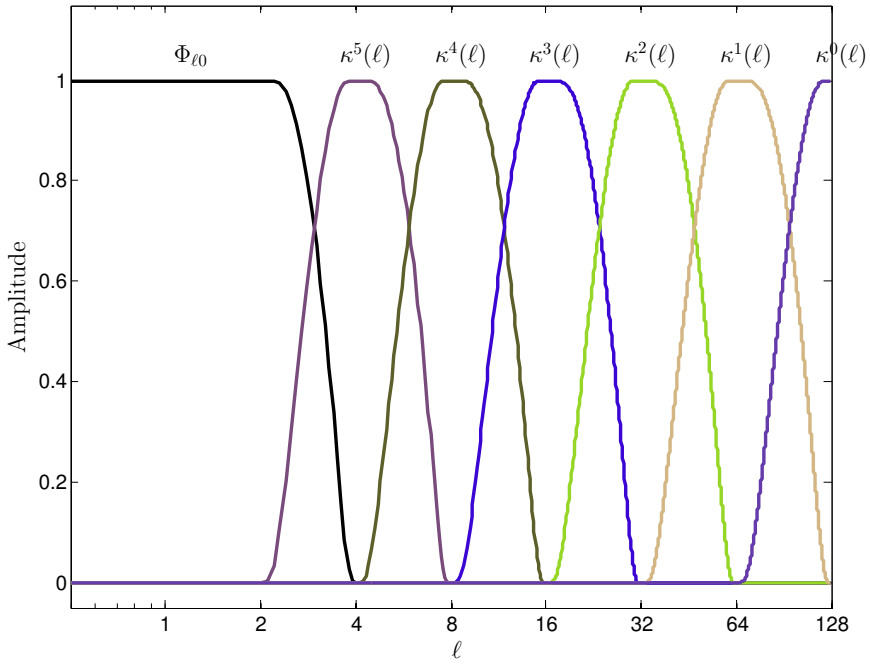

- Scale-discretised wavelet $\Psi^j \in \mathrm{L}^2(\mathbb{S}^2, \mathrm{d}\Omega)$ defined in harmonic space:

$$\Psi^j_{\ell m} \equiv \kappa^j(\ell) s_{\ell m} \, .$$

- Admissible wavelets constructed to satisfy a resolution of the identity:

$$|\Phi_{\ell 0}|^2 + \sum_{j=0}^{J} \sum_{m=-\ell}^{\ell} |\Psi^j_{\ell m}|^2 = 1 \, , \quad \forall \ell \, .$$

scaling function — wavelet

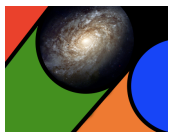

Scale-discretised wavelets on the sphere

Wavelets

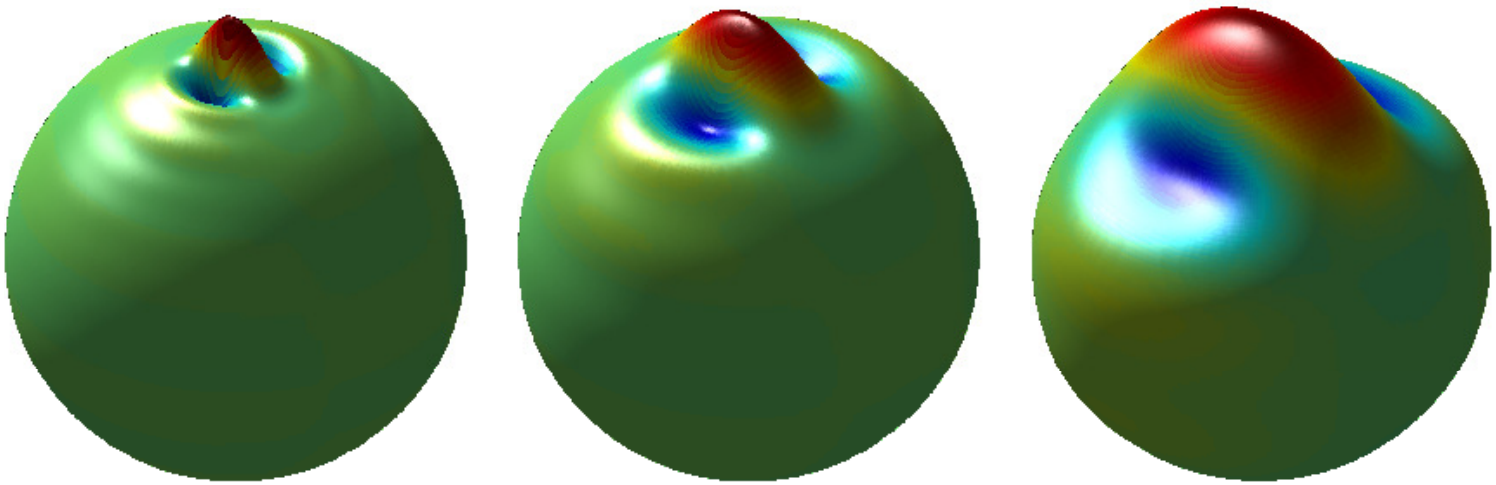

(a) $j = 4$ (b) $j = 3$ (c) $j = 2$

Figure: Scale-discretised wavelets on the sphere.

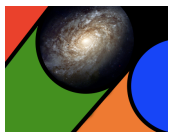

Scale-discretised wavelets on the sphere

Forward and inverse transform (*i.e.* analysis and synthesis)

- The scale-discretised wavelet transform is given by the usual projection onto each wavelet:

$$W^{\Psi^j}(\rho) = \langle f,\, \mathcal{R}_\rho \Psi^j \rangle = \int_{\mathbb{S}^2} \mathrm{d}\Omega(\omega) f(\omega) (\mathcal{R}_\rho \Psi^j)^*(\omega) \,.$$

projection

- The original function may be recovered exactly in practice from the wavelet (and scaling) coefficients:

$$f(\omega) = 2\pi \int_{\mathbb{S}^2} \mathrm{d}\Omega(\omega') W^\Phi(\omega') (\mathcal{R}_{\omega'} L^{\mathrm{d}} \Phi)(\omega) + \sum_{j=0}^{J} \int_{\mathrm{SO}(3)} \mathrm{d}\varrho(\rho) W^{\Psi^j}(\rho) (\mathcal{R}_\rho L^{\mathrm{d}} \Psi^j)(\omega) \,.$$

scaling function contribution; finite sum; wavelet contribution

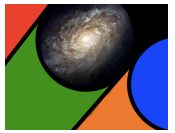

Scale-discretised wavelets on the sphere

Forward and inverse transform (*i.e.* analysis and synthesis)

- The scale-discretised wavelet transform is given by the usual projection onto each wavelet:

$$W^{\Psi^j}(\rho) = \langle f,\, \mathcal{R}_\rho \Psi^j \rangle = \int_{\mathbb{S}^2} \mathrm{d}\Omega(\omega) f(\omega) (\mathcal{R}_\rho \Psi^j)^*(\omega) \,.$$

projection

- The original function may be recovered exactly in practice from the wavelet (and scaling) coefficients:

$$f(\omega) = 2\pi \int_{\mathbb{S}^2} \mathrm{d}\Omega(\omega') W^{\Phi}(\omega') (\mathcal{R}_{\omega'} L^{\mathrm{d}} \Phi)(\omega) + \sum_{j=0}^{J} \int_{\mathrm{SO}(3)} \mathrm{d}\varrho(\rho) W^{\Psi^j}(\rho) (\mathcal{R}_\rho L^{\mathrm{d}} \Psi^j)(\omega) \,.$$

scaling function contribution; finite sum; wavelet contribution

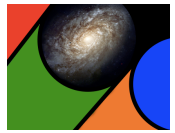

Scale-discretised wavelets on the sphere

Exact and efficient computation

- Wavelet analysis can be posed as an inverse Wigner transform on $\mathrm{SO}(3)$:

$$W^{\Psi^j}(\rho) = \sum_{\ell=0}^{L-1} \sum_{m=-\ell}^{\ell} \sum_{n=-\ell}^{\ell} \frac{2\ell+1}{8\pi^2} \left(W^{\Psi^j}\right)^{\ell}_{mn} D^{\ell *}_{mn}(\rho) \,, \quad \text{where} \quad \left(W^{\Psi^j}\right)^{\ell}_{mn} = \frac{8\pi^2}{2\ell+1} f_{\ell m} \Psi^{j*}_{\ell n} \,.$$

which can be computed efficiently via a factoring of rotations (Risbo 1996, Wandelt & Gorski 2001, McEwen *et al.* 2007).

- Wavelet synthesis can be posed as an forward Wigner transform on $\mathrm{SO}(3)$:

$$f(\omega) \sim \sum_{j=0}^{J} \int_{\mathrm{SO}(3)} \mathrm{d}\varrho(\rho) W^{\Psi^j}(\rho) (\mathcal{R}_\rho L^{\mathrm{d}} \Psi^j)(\omega) = \sum_{j=0}^{J} \sum_{\ell mn} \frac{2\ell+1}{8\pi^2} \left(W^{\Psi^j}\right)^{\ell}_{mn} \Psi^j_{\ell n} Y_{\ell m}(\omega) \,,$$

where

$$\left(W^{\Psi^j}\right)^{\ell}_{mn} = \langle W^{\Psi^j}, D^{\ell *}_{mn} \rangle = \int_{\mathrm{SO}(3)} \mathrm{d}\varrho(\rho) W^{\Psi^j}(\rho) D^{\ell}_{mn}(\rho) \,,$$

which can be computed efficiently via a factoring of rotations (Risbo 1996, Wiaux, McEwen *et al.* 2008) and exactly by employing the Driscoll & Healy (1994) or McEwen & Wiaux (2011) sampling theorem.

Scale-discretised wavelets on the sphere

Exact and efficient computation

- Wavelet analysis can be posed as an inverse Wigner transform on $\mathrm{SO}(3)$:

$$W^{\Psi^j}(\rho) = \sum_{\ell=0}^{L-1} \sum_{m=-\ell}^{\ell} \sum_{n=-\ell}^{\ell} \frac{2\ell+1}{8\pi^2} \left(W^{\Psi^j}\right)^{\ell}_{mn} D^{\ell *}_{mn}(\rho) \,, \quad \text{where} \quad \left(W^{\Psi^j}\right)^{\ell}_{mn} = \frac{8\pi^2}{2\ell+1} f_{\ell m} \Psi^{j*}_{\ell n} \,.$$

  which can be computed efficiently via a factoring of rotations (Risbo 1996, Wandelt & Gorski 2001, McEwen *et al.* 2007).

- Wavelet synthesis can be posed as an forward Wigner transform on $\mathrm{SO}(3)$:

$$f(\omega) \sim \sum_{j=0}^{J} \int_{\mathrm{SO}(3)} \mathrm{d}\varrho(\rho) W^{\Psi^j}(\rho) (\mathcal{R}_\rho L^{\mathrm{d}} \Psi^j)(\omega) = \sum_{j=0}^{J} \sum_{\ell mn} \frac{2\ell+1}{8\pi^2} \left(W^{\Psi^j}\right)^{\ell}_{mn} \Psi^{j}_{\ell n} Y_{\ell m}(\omega) \,,$$

  where

$$\left(W^{\Psi^j}\right)^{\ell}_{mn} = \langle W^{\Psi^j}, D^{\ell *}_{mn} \rangle = \int_{\mathrm{SO}(3)} \mathrm{d}\varrho(\rho) W^{\Psi^j}(\rho) D^{\ell}_{mn}(\rho) \,,$$

  which can be computed efficiently via a factoring of rotations (Risbo 1996, Wiaux, McEwen *et al.* 2008) and exactly by employing the Driscoll & Healy (1994) or McEwen & Wiaux (2011) sampling theorem.

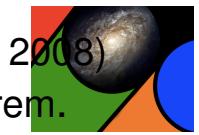

Scale-discretised wavelets on the sphere

Exact and efficient computation

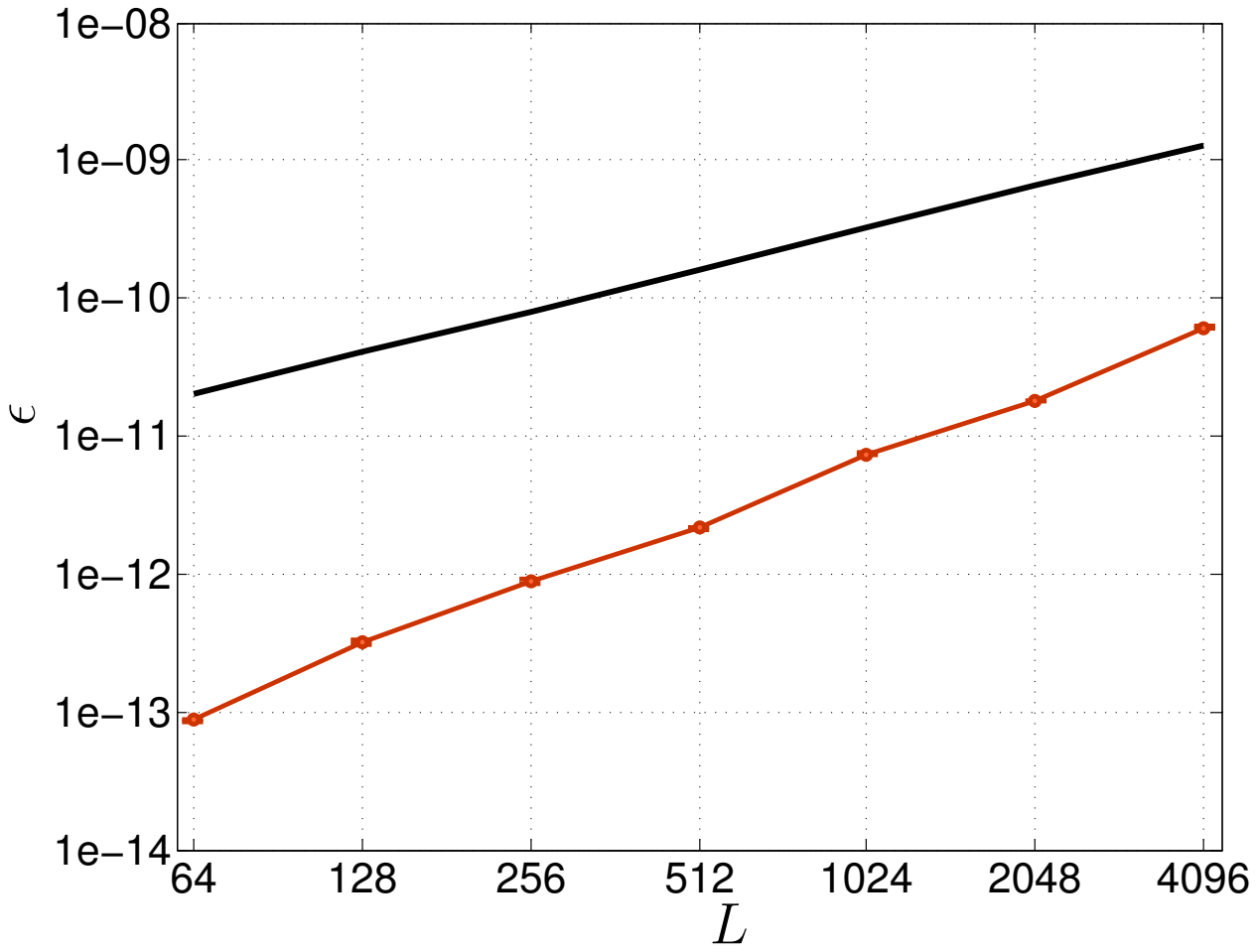

Figure: Numerical accuracy.

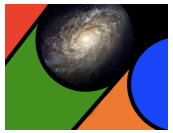

Scale-discretised wavelets on the sphere

Exact and efficient computation

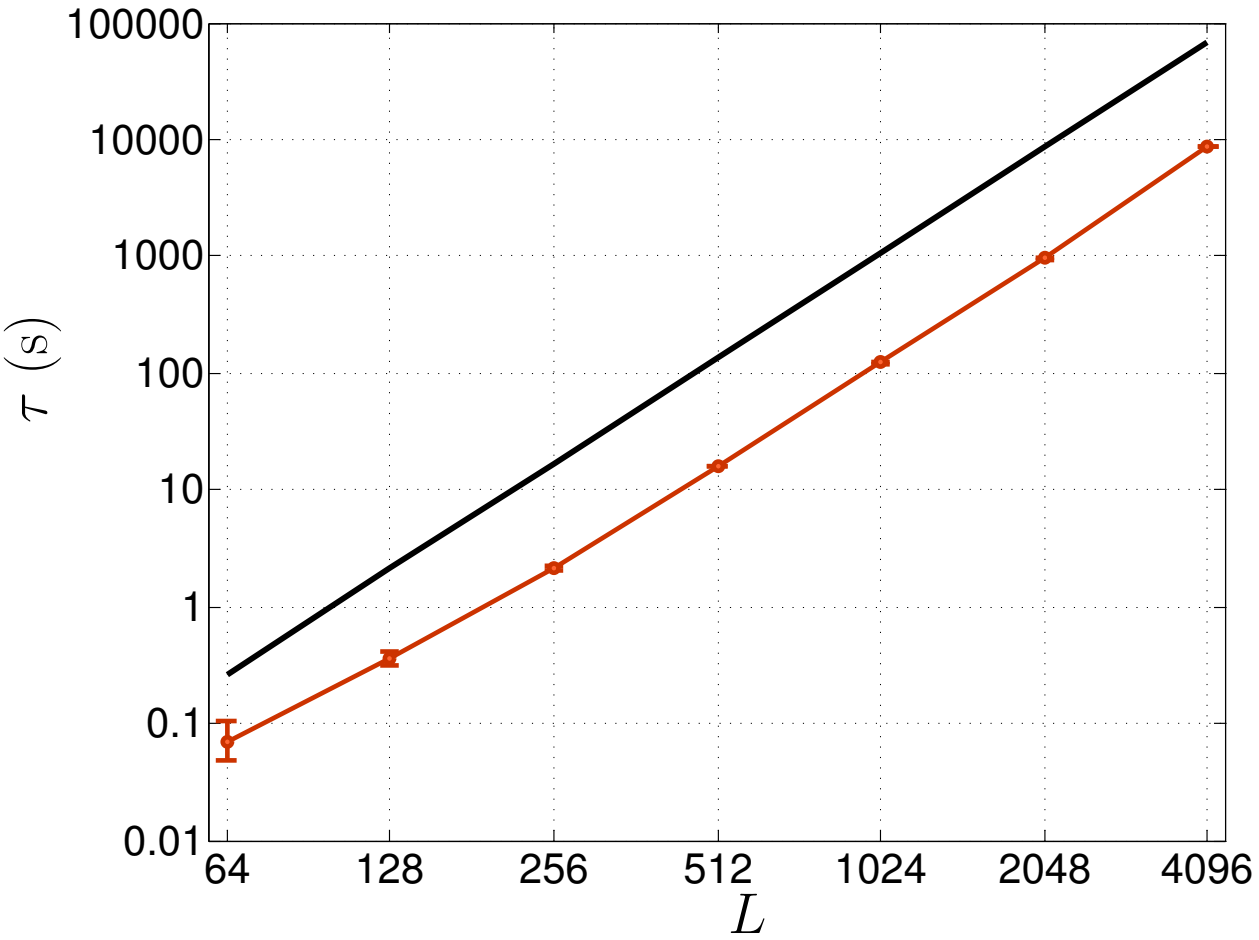

Figure: Computation time.

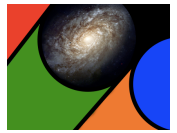

Scale-discretised wavelets on the sphere

Codes

S2DW code

http://www.s2dw.org

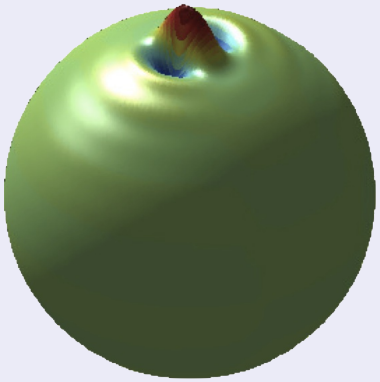

Exact reconstruction with directional wavelets on the sphere
Wiaux, McEwen, Vandergheynst, Blanc (2008)

- Fortran
- Parallelised
- Supports directional and steerable wavelets

S2LET code

http://www.s2let.org

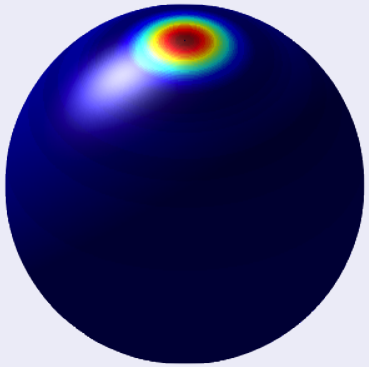

S2LET: A code to perform fast wavelet analysis on the sphere
Leistedt, McEwen, Vandergheynst, Wiaux (2012)

- C, Matlab, IDL, Java
- Supports only axisymmetric wavelets at present
- Future extensions planned (directional and steerable wavelets, faster algos, spin wavelets)

Scale-discretised wavelets on the sphere

Illustration

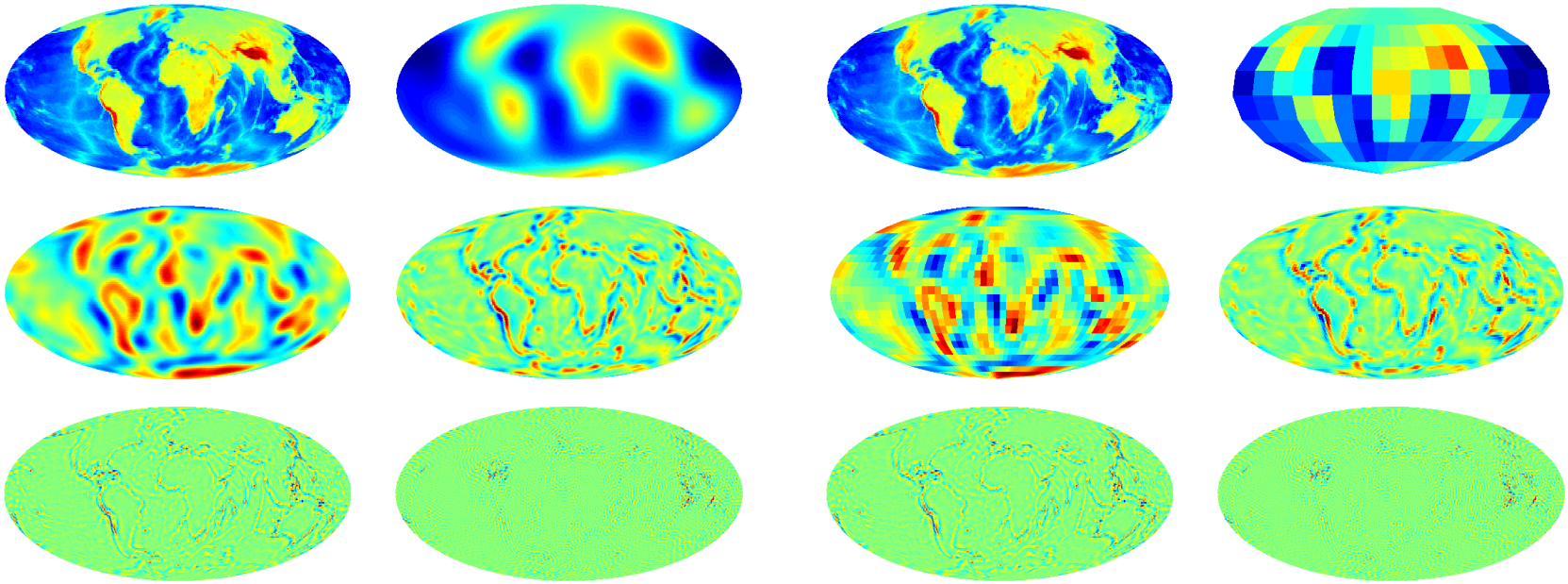

(a) Undecimated (b) Multi-resolution

Figure: Scale-discretised wavelet transform of a topography map of the Earth.

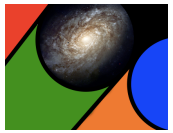

Motivation for using wavelets to detect cosmic strings

- Denote the wavelet coefficients of the data d by

$$W^d_{j\rho} = \langle d, \Psi_{j\rho} \rangle$$

  for scale $j \in \mathbb{Z}^+$ and position $\rho \in \mathrm{SO}(3)$.

- Consider an even azimuthal band-limit $N = 4$ to yield wavelet with odd azimuthal symmetry.

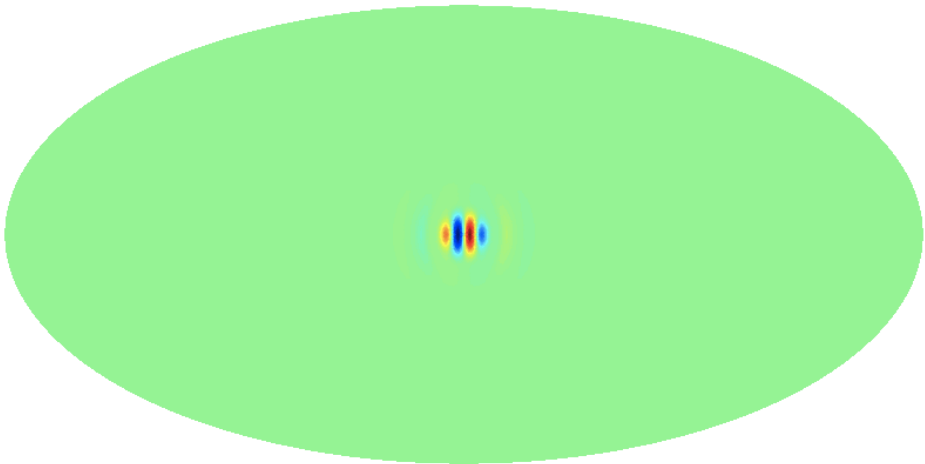

Figure: Example wavelet matched to the expected string contribution.

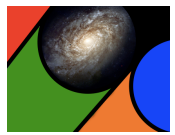

Motivation for using wavelets to detect cosmic strings

- Wavelet transform yields a sparse representation of the string signal $\rightarrow$ hope to effectively separate the CMB and string signal in wavelet space.

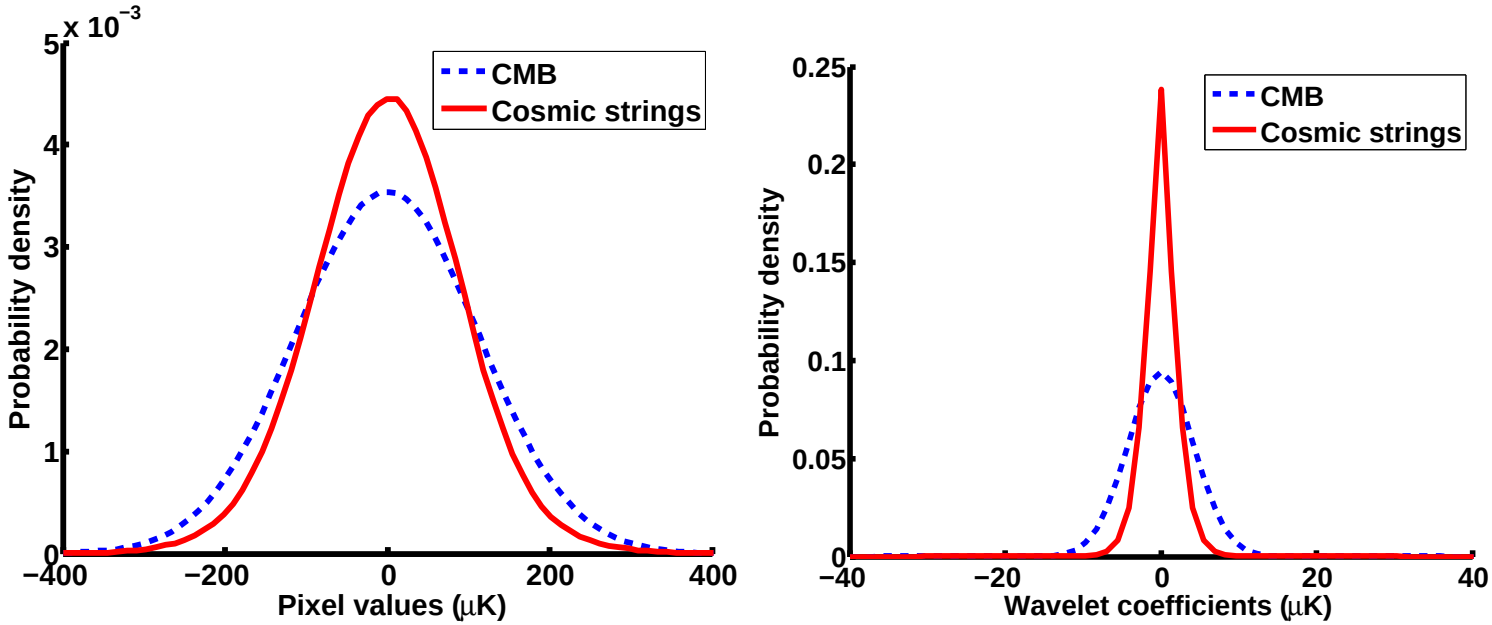

Figure: Distribution of CMB and string signal in pixel (left) and wavelet space (right).

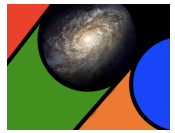

Learning the statistics of the CMB and string signals in wavelet space

- Wavelet-Bayesian approach to estimate the string tension and map:

$$\underbrace{d(\theta,\varphi)}_{\text{observation}} = \underbrace{c(\theta,\varphi)}_{\text{CMB}} + \underbrace{G\mu \cdot s(\theta,\varphi)}_{\text{strings}} .$$

- Need to determine statistical description of the CMB and string signals in wavelet space.
- Calculate analytically the probability distribution of the CMB in wavelet space.
- Fit a generalised Gaussian distribution (GGD) for the wavelet coefficients of a string training map (*cf.* Wiaux *et al.* 2009):

$$\mathrm{P}_j^s(W_{j\rho}^s \,|\, G\mu) = \frac{\upsilon_j}{2G\mu\nu_j\Gamma(\upsilon_j{}^{-1})}\, \mathrm{e}^{\left(-\left|\frac{W_{j\rho}^s}{G\mu\nu_j}\right|^{\upsilon_j}\right)},$$

with scale parameter ν_j and shape parameter υ_j.

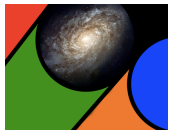

Learning the statistics of the CMB and string signals in wavelet space

- Wavelet-Bayesian approach to estimate the string tension and map:

$$\underbrace{d(\theta,\varphi)}_{\text{observation}} = \underbrace{c(\theta,\varphi)}_{\text{CMB}} + \underbrace{G\mu \cdot s(\theta,\varphi)}_{\text{strings}}.$$

- Need to determine statistical description of the CMB and string signals in wavelet space.
- Calculate analytically the probability distribution of the CMB in wavelet space.
- Fit a generalised Gaussian distribution (GGD) for the wavelet coefficients of a string training map (*cf.* Wiaux *et al.* 2009):

$$\mathrm{P}_j^s(W_{j\rho}^s \,|\, G\mu) = \frac{\upsilon_j}{2G\mu\nu_j\Gamma(\upsilon_j{}^{-1})}\, \mathrm{e}^{\left(-\left|\frac{W_{j\rho}^s}{G\mu\nu_j}\right|^{\upsilon_j}\right)},$$

with scale parameter ν_j and shape parameter υ_j.

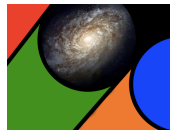

Learning the statistics of the CMB and string signals in wavelet space

- Wavelet-Bayesian approach to estimate the string tension and map:

$$\underbrace{d(\theta,\varphi)}_{\text{observation}} = \underbrace{c(\theta,\varphi)}_{\text{CMB}} + \underbrace{G\mu \cdot s(\theta,\varphi)}_{\text{strings}} .$$

- Need to determine statistical description of the CMB and string signals in wavelet space.
- Calculate analytically the probability distribution of the CMB in wavelet space.

- Fit a generalised Gaussian distribution (GGD) for the wavelet coefficients of a string training map (*cf.* Wiaux *et al.* 2009):

$$\mathrm{P}_j^s(W_{j\rho}^s \,|\, G\mu) = \frac{\upsilon_j}{2G\mu\nu_j\Gamma(\upsilon_j{}^{-1})}\, \mathrm{e}^{\left(-\left|\frac{W_{j\rho}^s}{G\mu\nu_j}\right|^{\upsilon_j}\right)},$$

with scale parameter ν_j and shape parameter υ_j.

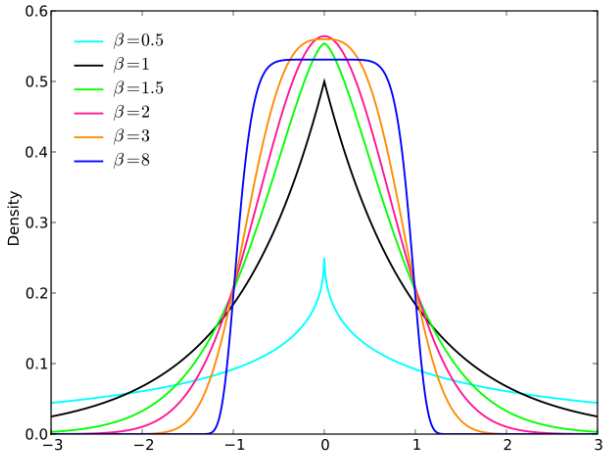

Figure: GGD

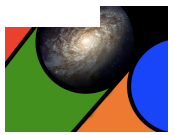

Learning the statistics of the CMB and string signals in wavelet space

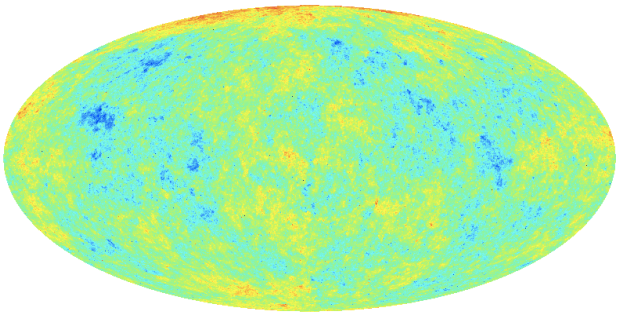

(a) String training map

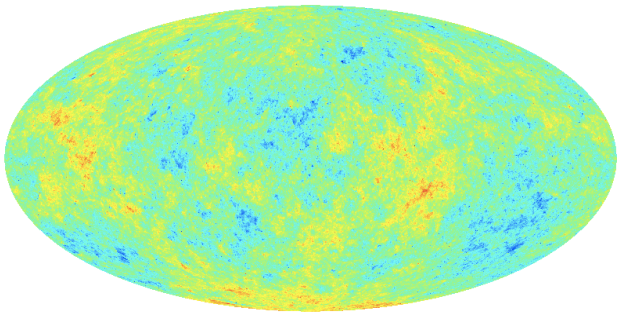

(b) String testing map

Figure: Cosmic string simulations.

- Distributions in close agreement.

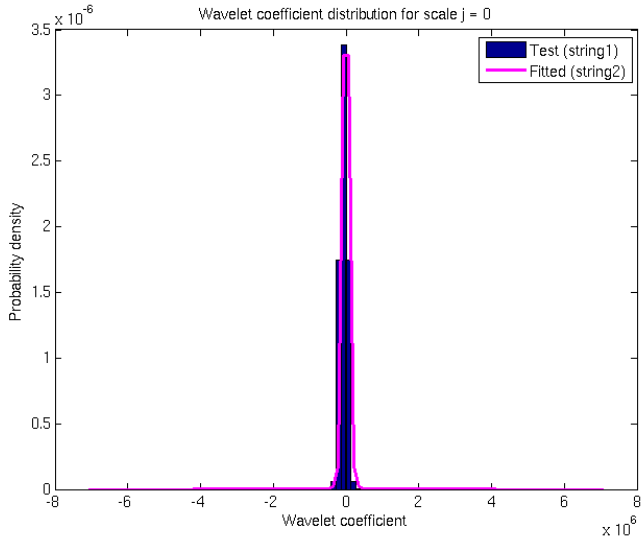

Figure: Distributions for wavelet scale $j = 0$.

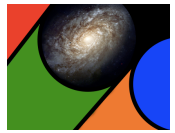

Learning the statistics of the CMB and string signals in wavelet space

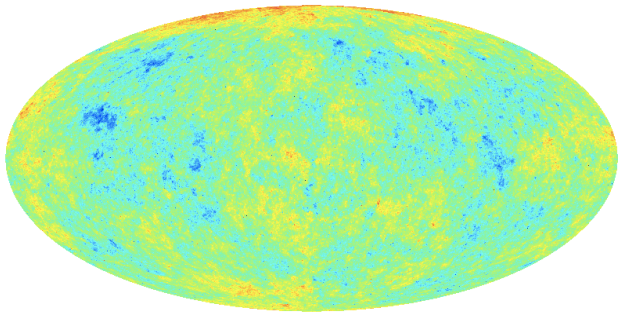

(a) String training map

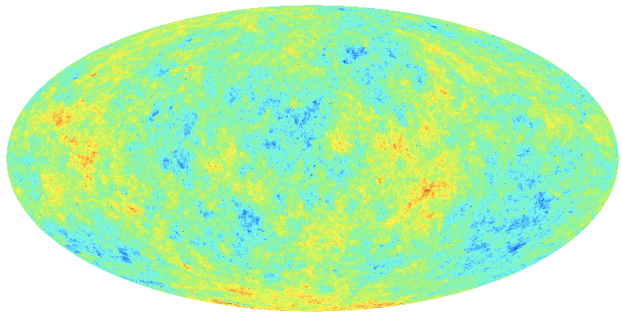

(b) String testing map

Figure: Cosmic string simulations.

- Distributions in close agreement.

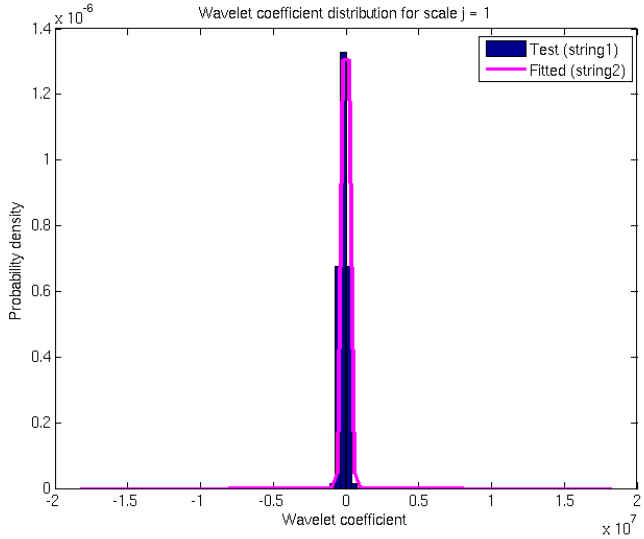

Figure: Distributions for wavelet scale $j = 1$.

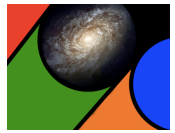

Learning the statistics of the CMB and string signals in wavelet space

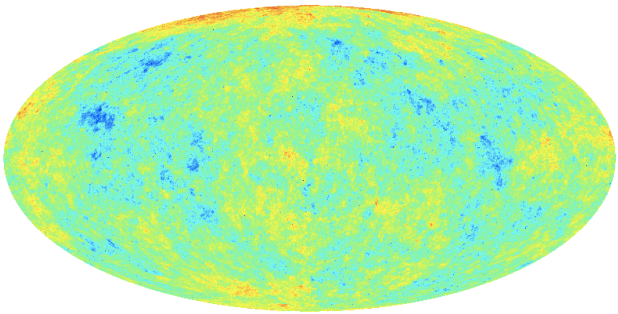

(a) String training map

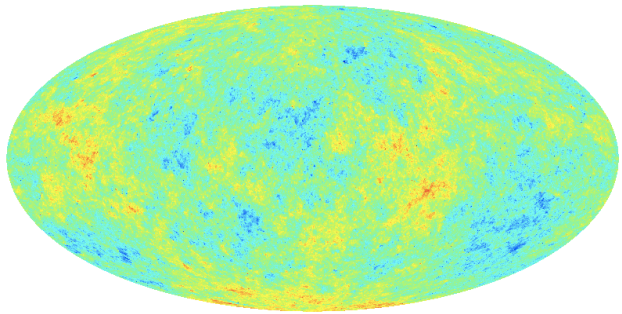

(b) String testing map

Figure: Cosmic string simulations.

- Distributions in close agreement.

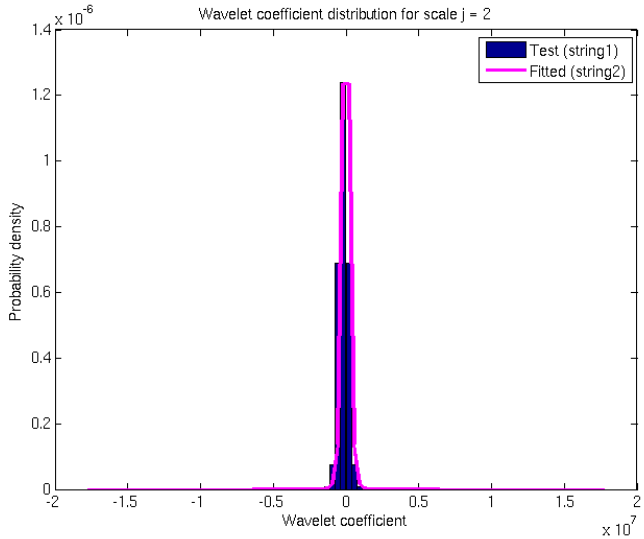

Figure: Distributions for wavelet scale $j = 2$.

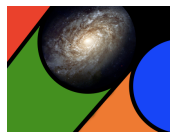

Learning the statistics of the CMB and string signals in wavelet space

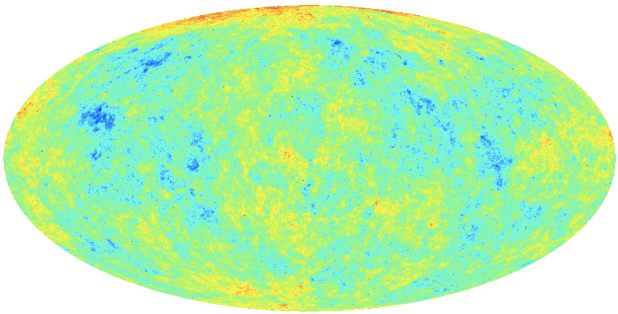

(a) String training map

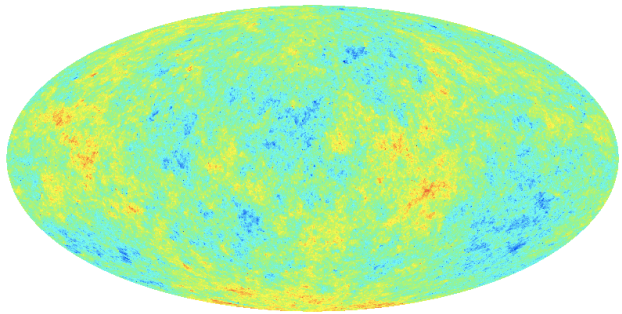

(b) String testing map

Figure: Cosmic string simulations.

- Distributions in close agreement.

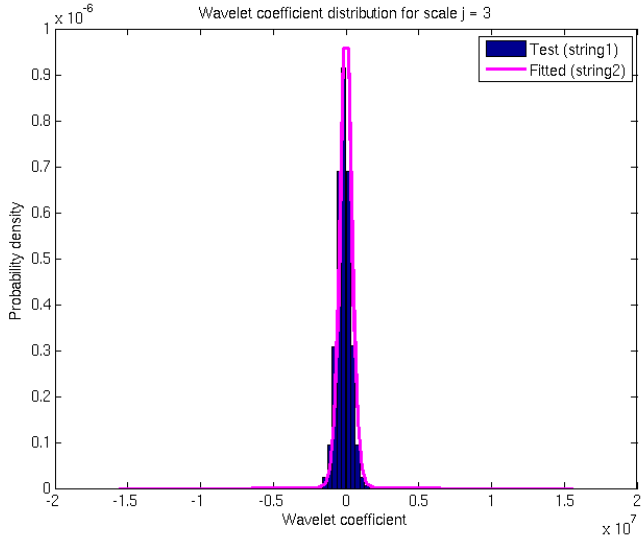

Figure: Distributions for wavelet scale $j = 3$.

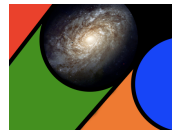

Learning the statistics of the CMB and string signals in wavelet space

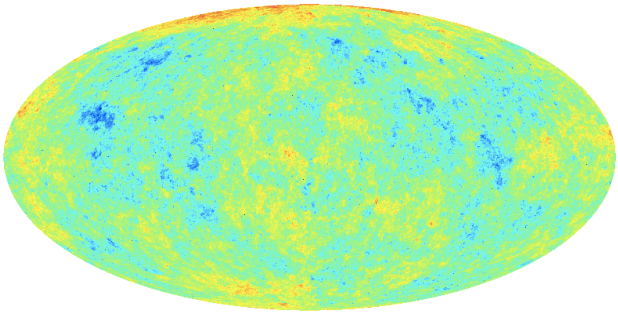

(a) String training map

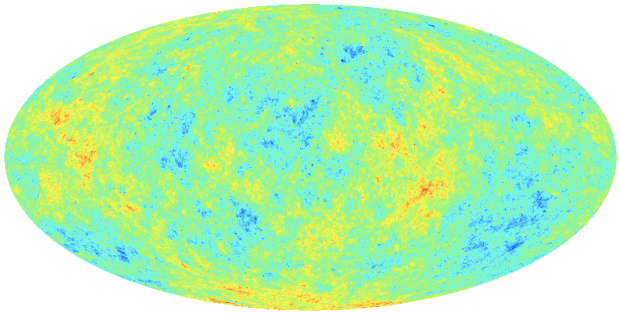

(b) String testing map

Figure: Cosmic string simulations.

- Distributions in close agreement.
- Accurately characterised statistics of string signals in wavelet space.

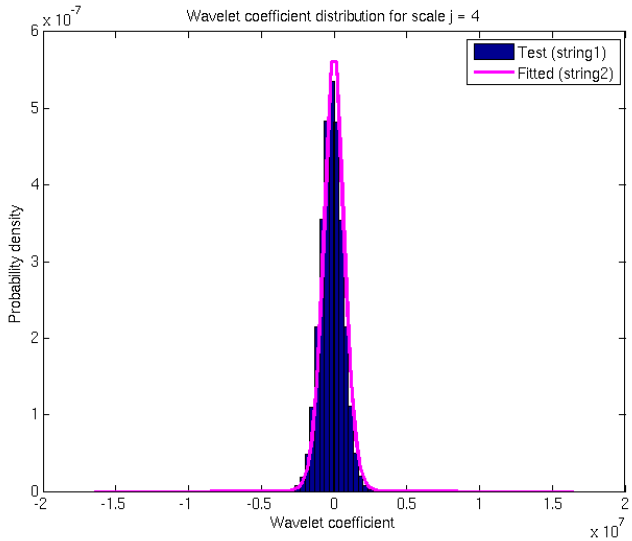

Figure: Distributions for wavelet scale $j = 4$.

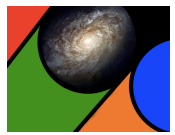

Spherical wavelet-Bayesian string tension estimation

- Perform Bayesian string tension estimation in wavelet space.
- For each wavelet coefficient the likelihood is given by

$$\mathrm{P}(W^d_{j\rho} \,|\, G\mu) = \mathrm{P}(W^s_{j\rho} + W^c_{j\rho} \,|\, G\mu) = \int_{\mathbb{R}} \mathrm{d}W^s_{j\rho}\, \mathrm{P}^c_j(W^d_{j\rho} - W^s_{j\rho})\, \mathrm{P}^s_j(W^s_{j\rho} \,|\, G\mu)\,.$$

- The overall likelihood of the data is given by

$$\mathrm{P}(W^d \,|\, G\mu) = \prod_{j,\rho} \mathrm{P}(W^d_{j\rho} \,|\, G\mu)\,,$$

where we have assumed independence for numerical tractability.

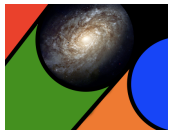

Spherical wavelet-Bayesian string tension estimation

- Perform Bayesian string tension estimation in wavelet space.
- For each wavelet coefficient the likelihood is given by

$$\mathrm{P}(W^d_{j\rho} \,|\, G\mu) = \mathrm{P}(W^s_{j\rho} + W^c_{j\rho} \,|\, G\mu) = \int_{\mathbb{R}} \mathrm{d}W^s_{j\rho}\, \mathrm{P}^c_j(W^d_{j\rho} - W^s_{j\rho})\, \mathrm{P}^s_j(W^s_{j\rho} \,|\, G\mu)\,.$$

- The overall likelihood of the data is given by

$$\mathrm{P}(W^d \,|\, G\mu) = \prod_{j,\rho} \mathrm{P}(W^d_{j\rho} \,|\, G\mu)\,,$$

where we have assumed independence for numerical tractability.

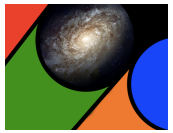

Spherical wavelet-Bayesian string tension estimation

- Perform Bayesian string tension estimation in wavelet space.
- For each wavelet coefficient the likelihood is given by

$$\mathrm{P}(W^d_{j\rho} \,|\, G\mu) = \mathrm{P}(W^s_{j\rho} + W^c_{j\rho} \,|\, G\mu) = \int_{\mathbb{R}} \mathrm{d}W^s_{j\rho}\, \mathrm{P}^c_j(W^d_{j\rho} - W^s_{j\rho})\, \mathrm{P}^s_j(W^s_{j\rho} \,|\, G\mu)\,.$$

- The overall likelihood of the data is given by

$$\mathrm{P}(W^d \,|\, G\mu) = \prod_{j,\rho} \mathrm{P}(W^d_{j\rho} \,|\, G\mu)\,,$$

where we have assumed independence for numerical tractability.

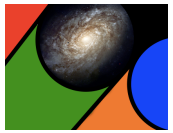

Spherical wavelet-Bayesian string tension estimation

- Compute the string tension posterior $\mathrm{P}(G\mu \mid W^d)$ by Bayes theorem:

$$\mathrm{P}(G\mu \mid W^d) = \frac{\mathrm{P}(W^d \mid G\mu)\,\mathrm{P}(G\mu)}{\mathrm{P}(W^d)} \propto \mathrm{P}(W^d \mid G\mu)\,\mathrm{P}(G\mu)\,.$$

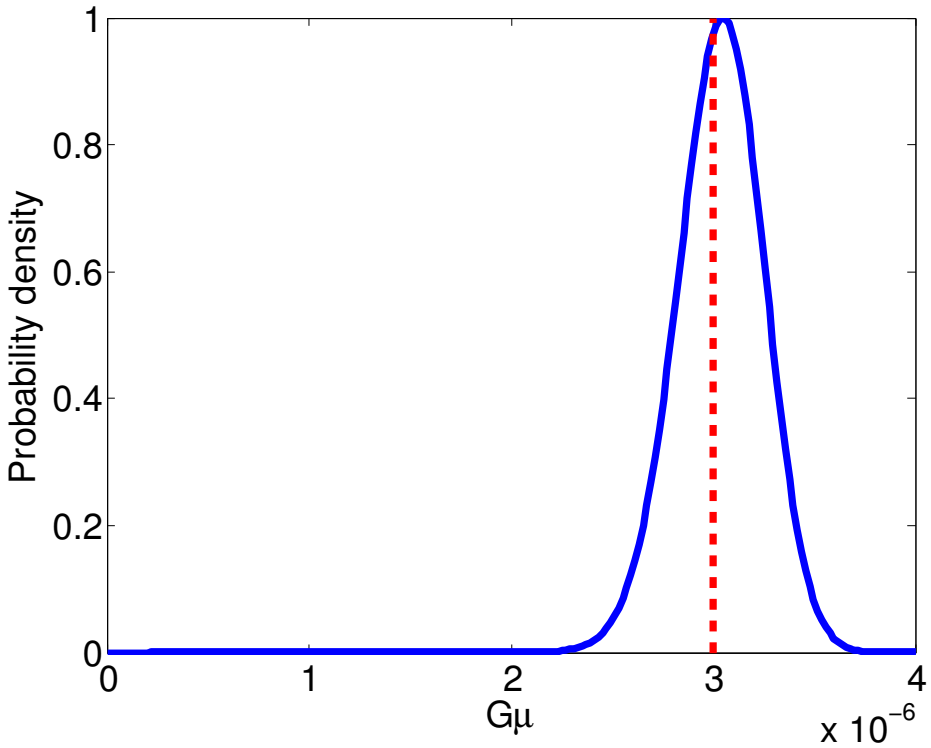

Figure: Posterior distribution of the string tension (true $G\mu = 3 \times 10^{-6}$).

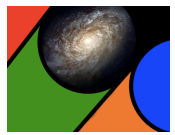

Spherical wavelet-Bayesian string tension estimation

- Compute the string tension posterior $\mathrm{P}(G\mu \mid W^d)$ by Bayes theorem:

$$\mathrm{P}(G\mu \mid W^d) = \frac{\mathrm{P}(W^d \mid G\mu)\,\mathrm{P}(G\mu)}{\mathrm{P}(W^d)} \propto \mathrm{P}(W^d \mid G\mu)\,\mathrm{P}(G\mu)\ .$$

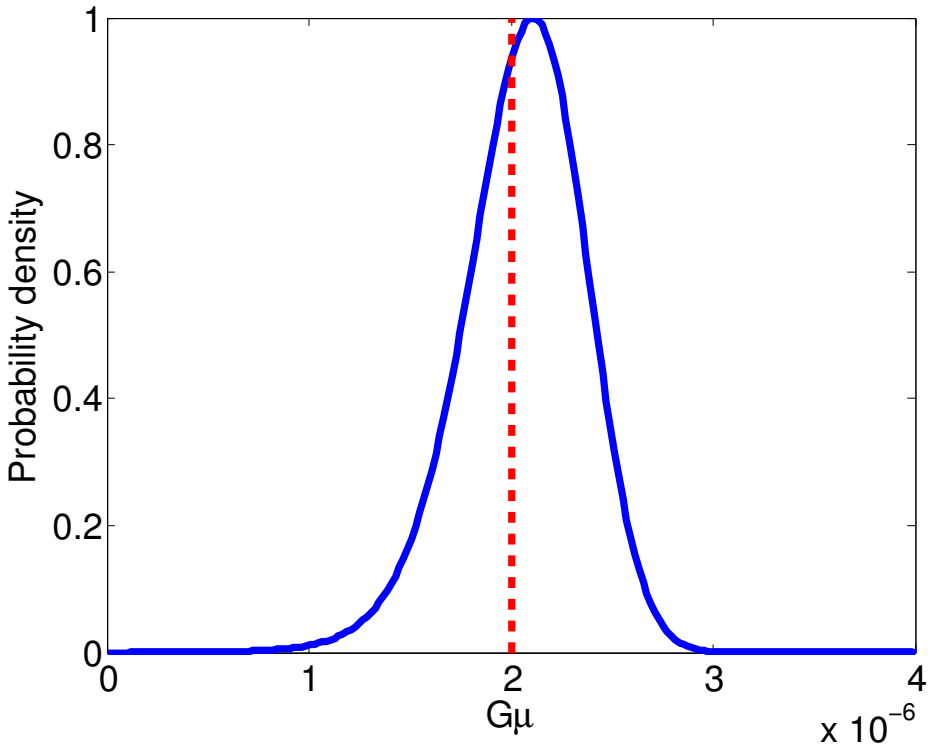

Figure: Posterior distribution of the string tension (true $G\mu = 2 \times 10^{-6}$).

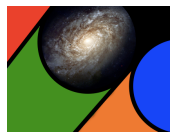

Spherical wavelet-Bayesian string tension estimation

- Compute the string tension posterior $\mathrm{P}(G\mu \mid W^d)$ by Bayes theorem:

$$\mathrm{P}(G\mu \mid W^d) = \frac{\mathrm{P}(W^d \mid G\mu)\,\mathrm{P}(G\mu)}{\mathrm{P}(W^d)} \propto \mathrm{P}(W^d \mid G\mu)\,\mathrm{P}(G\mu)\,.$$

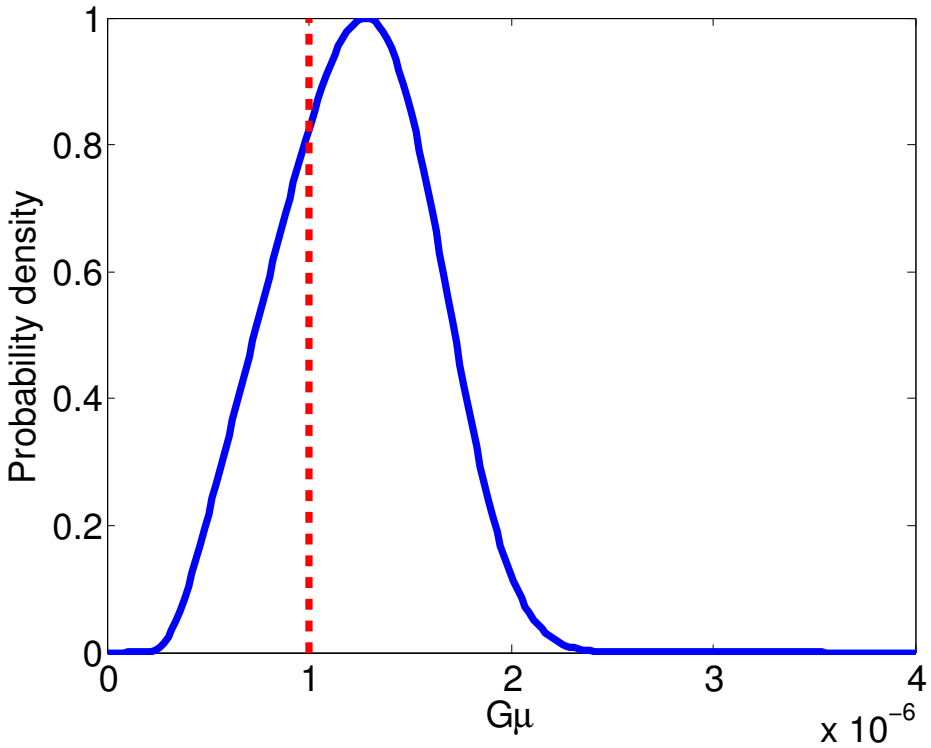

Figure: Posterior distribution of the string tension (true $G\mu = 1 \times 10^{-6}$).

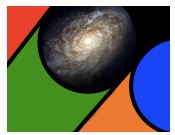

Bayesian evidence for strings

- Compute Bayesian evidences to compare the string model M^s to the alternative model M^c that the observed data is comprised of just a CMB contribution.
- The Bayesian evidence of the string model is given by

$$E^s = \mathrm{P}(W^d \,|\, \mathrm{M}^s) = \int_{\mathbb{R}} \mathrm{d}(G\mu)\, \mathrm{P}(W^d \,|\, G\mu)\, \mathrm{P}(G\mu)\ .$$

- The Bayesian evidence of the CMB model is given by

$$E^c = \mathrm{P}(W^d \,|\, \mathrm{M}^c) = \prod_{j,\rho} \mathrm{P}^c_j(W^d_{j\rho})\ .$$

- Compute the Bayes factor to determine the preferred model:

$$\Delta \ln E = \ln(E^s/E^c)\ .$$

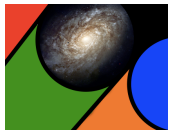

Bayesian evidence for strings

- Compute Bayesian evidences to compare the string model M^s to the alternative model M^c that the observed data is comprised of just a CMB contribution.
- The Bayesian evidence of the string model is given by

$$E^s = \mathrm{P}(W^d \,|\, \mathrm{M}^s) = \int_{\mathbb{R}} \mathrm{d}(G\mu)\, \mathrm{P}(W^d \,|\, G\mu)\, \mathrm{P}(G\mu)\ .$$

- The Bayesian evidence of the CMB model is given by

$$E^c = \mathrm{P}(W^d \,|\, \mathrm{M}^c) = \prod_{j,\rho} \mathrm{P}^c_j(W^d_{j\rho})\ .$$

- Compute the Bayes factor to determine the preferred model:

$$\Delta \ln E = \ln(E^s/E^c)\ .$$

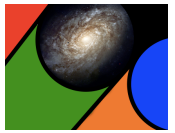

Bayesian evidence for strings

- Compute Bayesian evidences to compare the string model M^s to the alternative model M^c that the observed data is comprised of just a CMB contribution.
- The Bayesian evidence of the string model is given by

$$E^s = \mathrm{P}(W^d \,|\, \mathrm{M}^s) = \int_{\mathbb{R}} \mathrm{d}(G\mu)\, \mathrm{P}(W^d \,|\, G\mu)\, \mathrm{P}(G\mu)\ .$$

- The Bayesian evidence of the CMB model is given by

$$E^c = \mathrm{P}(W^d \,|\, \mathrm{M}^c) = \prod_{j,\rho} \mathrm{P}^c_j(W^d_{j\rho})\ .$$

- Compute the Bayes factor to determine the preferred model:

$$\Delta \ln E = \ln(E^s/E^c)\ .$$

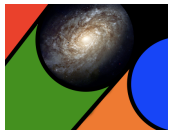

Bayesian evidence for strings

- Compute Bayesian evidences to compare the string model M^s to the alternative model M^c that the observed data is comprised of just a CMB contribution.
- The Bayesian evidence of the string model is given by

$$E^s = \mathrm{P}(W^d \,|\, \mathrm{M}^s) = \int_{\mathbb{R}} \mathrm{d}(G\mu)\, \mathrm{P}(W^d \,|\, G\mu)\, \mathrm{P}(G\mu)\ .$$

- The Bayesian evidence of the CMB model is given by

$$E^c = \mathrm{P}(W^d \,|\, \mathrm{M}^c) = \prod_{j,\rho} \mathrm{P}^c_j(W^d_{j\rho})\ .$$

- Compute the Bayes factor to determine the preferred model:

$$\Delta \ln E = \ln(E^s/E^c)\ .$$

Table: Tension estimates and log-evidence differences for simulations.

$G\mu/10^{-6}$	0.7	0.8	0.9	1.0	2.0	3.0
$\widehat{G\mu}/10^{-6}$	1.1	1.2	1.2	1.3	2.1	3.1
$\Delta \ln E$	-1.3	-1.1	-0.9	-0.7	5.5	29

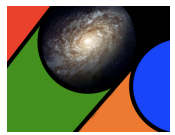

Recovering string maps

- Inference of the wavelet coefficients of the underlying string map encoded in posterior probability distribution $\mathrm{P}(W^s_{j\rho} \mid W^d)$.
- Estimate the wavelet coefficients of the string map from the mean of the posterior distribution:

$$\overline{W}^s_{j\rho} = \int_{\mathbb{R}} \mathrm{d}W^s_{j\rho}\, W^s_{j\rho}\, \mathrm{P}(W^s_{j\rho} \mid W^d)$$

- Recover the string map from its wavelets (possible since the scale-discretised wavelet transform on the sphere supports exact reconstruction).
- Work in progress...

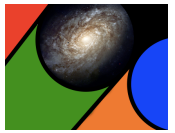

Recovering string maps

- Inference of the wavelet coefficients of the underlying string map encoded in posterior probability distribution $\mathrm{P}(W^s_{j\rho} \mid W^d)$.
- Estimate the wavelet coefficients of the string map from the mean of the posterior distribution:

$$\overline{W}^s_{j\rho} = \int_{\mathbb{R}} \mathrm{d}W^s_{j\rho}\, W^s_{j\rho}\, \mathrm{P}(W^s_{j\rho} \mid W^d)$$

- Recover the string map from its wavelets (possible since the scale-discretised wavelet transform on the sphere supports exact reconstruction).
- Work in progress...

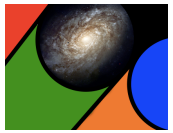

Outline

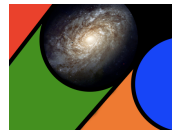

Bianchi VII_h cosmologies

Test fundamental assumptions on which modern cosmology is based, *e.g.* isotropy.

- Relax assumptions about the global structure of spacetime by allowing anisotropy about each point in the universe, *i.e.* rotation and shear.
- Yields more general solutions to Einstein's field equations $\rightarrow$ Bianchi cosmologies.
- Induces a characteristic subdominant, deterministic signature in the CMB, which is embedded in the usual stochastic anisotropies (Collins & Hawking 1973, Barrow *et al.* 1985).

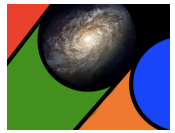

Bianchi VII_h cosmologies

Test fundamental assumptions on which modern cosmology is based, *e.g.* isotropy.

- Relax assumptions about the global structure of spacetime by allowing anisotropy about each point in the universe, *i.e.* rotation and shear.
- Yields more general solutions to Einstein's field equations $\rightarrow$ Bianchi cosmologies.
- Induces a characteristic subdominant, deterministic signature in the CMB, which is embedded in the usual stochastic anisotropies (Collins & Hawking 1973, Barrow *et al.* 1985).

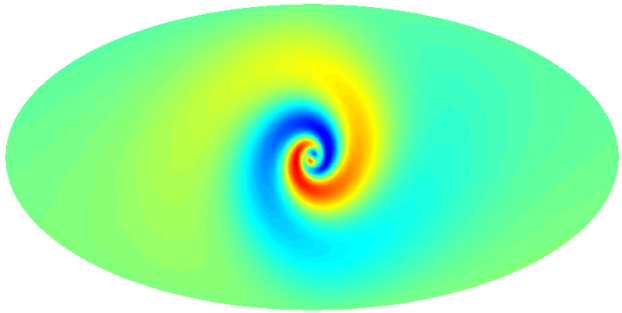

Figure: Bianchi CMB contribution.

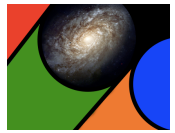

Bianchi VII_h cosmologies

Parameters

- Models described by the parameter vector:

$$\Theta_{\mathrm{B}} = \left(\Omega_{\mathrm{m}},\, \Omega_{\Lambda},\, x,\, (\omega/H)_0,\, \alpha, \beta, \gamma\right) .$$

- Free parameter, x, describing the comoving length-scale over which the principal axes of shear and rotation change orientation, *i.e.* 'spiralness'.
- Amplitude characterised by the dimensionless vorticity $(\omega/H)_0$, which influences the amplitude of the induced temperature contribution only and not its morphology.
- The orientation and handedness of the coordinate system is also free.

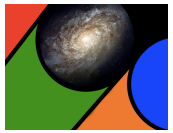

Bianchi VII_h cosmologies

Simulations

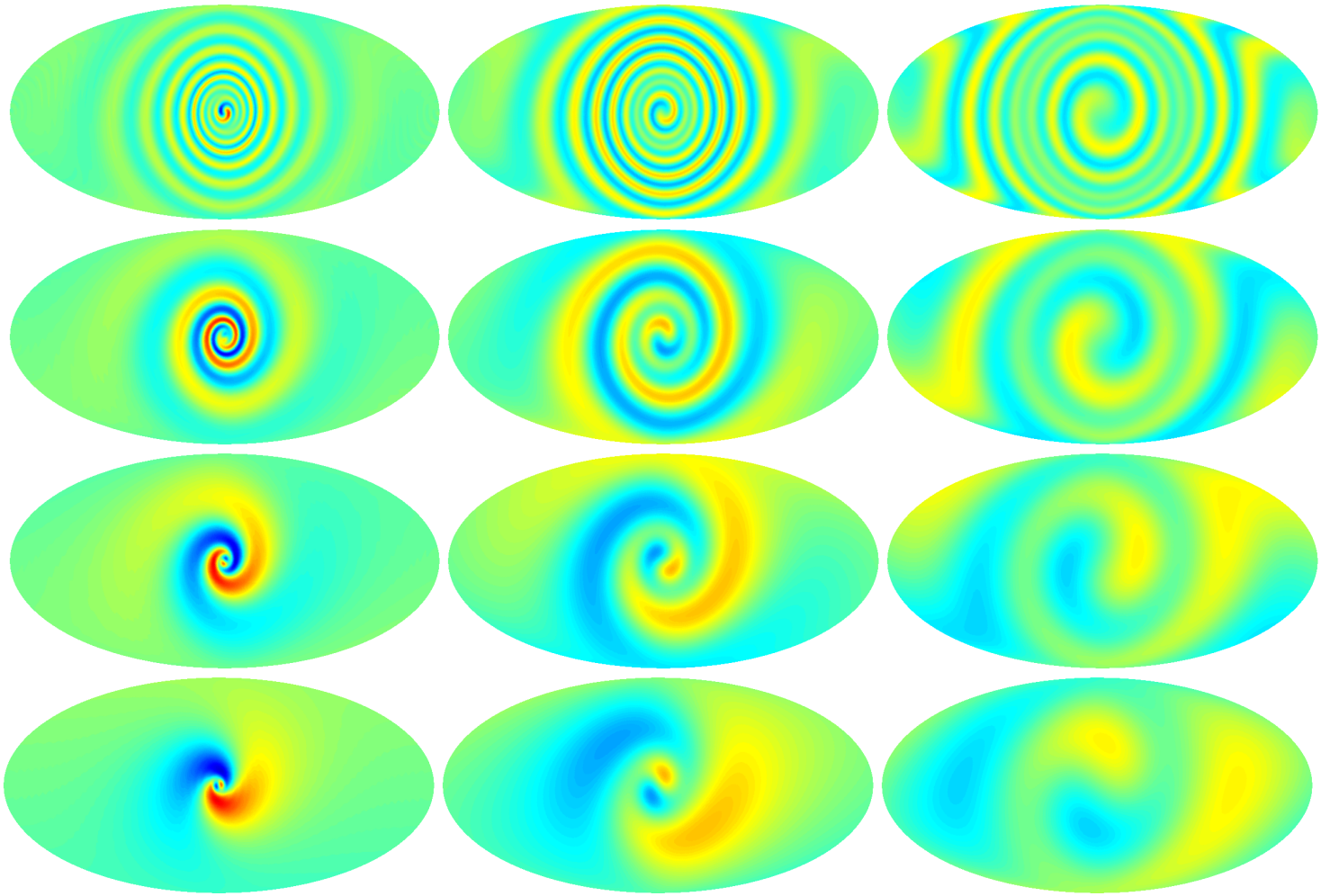

Figure: Simulated CMB contributions in Bianchi VII_h cosmologies for varying parameters.

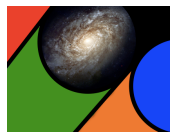

Bayesian analysis of Bianchi VII$_h$ cosmologies

Parameter estimation

- Perform Bayesian analysis of McEwen *et al.* (2013).
- Consider open and flat cosmologies with cosmological parameters:
  $\Theta_{\rm C} = (A_s,\, n_s,\, \tau,\, \Omega_{\rm b}h^2,\, \Omega_{\rm c}h^2,\, \Omega_\Lambda,\, \Omega_k)$.
- Recall Bianchi parameters:
  $\Theta_{\rm B} = \left(\Omega_{\rm m},\, \Omega_\Lambda,\, x,\, (\omega/H)_0,\, \alpha, \beta, \gamma\right)$.
- Likelihood given by

$$\mathrm{P}(\boldsymbol{d} \,|\, \Theta_{\rm B}, \Theta_{\rm C}) \propto \frac{1}{\sqrt{|\mathbf{X}(\Theta_{\rm C})|}} \mathrm{e}^{\left[-\chi^2(\Theta_{\rm C},\Theta_{\rm B})/2\right]},$$

where

$$\chi^2(\Theta_{\rm C},\Theta_{\rm B}) = \left[\boldsymbol{d} - \boldsymbol{b}(\Theta_{\rm B})\right]^\dagger \mathbf{X}^{-1}(\Theta_{\rm C}) \left[\boldsymbol{d} - \boldsymbol{b}(\Theta_{\rm B})\right].$$

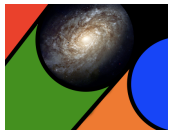

Bayesian analysis of Bianchi VII$_h$ cosmologies

Parameter estimation

- Perform Bayesian analysis of McEwen *et al.* (2013).
- Consider open and flat cosmologies with cosmological parameters:
  $\Theta_{\rm C} = (A_s,\, n_s,\, \tau,\, \Omega_{\rm b}h^2,\, \Omega_{\rm c}h^2,\, \Omega_\Lambda,\, \Omega_k)$.
- Recall Bianchi parameters:
  $\Theta_{\rm B} = \left(\Omega_{\rm m},\, \Omega_\Lambda,\, x,\, (\omega/H)_0,\, \alpha, \beta, \gamma\right)$.
- Likelihood given by

$$\mathrm{P}(\boldsymbol{d} \,|\, \Theta_{\rm B}, \Theta_{\rm C}) \propto \frac{1}{\sqrt{|\mathbf{X}(\Theta_{\rm C})|}} \mathrm{e}^{\left[-\chi^2(\Theta_{\rm C},\Theta_{\rm B})/2\right]},$$

where

$$\chi^2(\Theta_{\rm C},\Theta_{\rm B}) = \left[\boldsymbol{d} - \boldsymbol{b}(\Theta_{\rm B})\right]^\dagger \mathbf{X}^{-1}(\Theta_{\rm C}) \left[\boldsymbol{d} - \boldsymbol{b}(\Theta_{\rm B})\right].$$

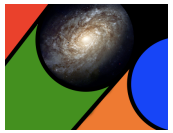

Bayesian analysis of Bianchi VII$_h$ cosmologies

Covariance

- Bianchi VII$_h$ templates can be computed accurately and rotated efficiently in harmonic space $\rightarrow$ consider harmonic space representation, where $\boldsymbol{d} = \{d_{\ell m}\}$ and $\boldsymbol{b}(\Theta_{\mathrm{B}}) = \{b_{\ell m}(\Theta_{\mathrm{B}})\}$.
- Partial-sky analysis that handles in harmonic space a mask applied in pixel space.
- Add masking noise in order to marginalise the pixel values of the data contained in the masked region, with variance for pixel i given by $\sigma_m^2(\omega_i)$.
- The covariance is then given by

$$\mathbf{X}(\Theta_{\mathrm{C}}) = \mathbf{C}(\Theta_{\mathrm{C}}) + \mathbf{M}\,,$$

where

  - $\mathbf{C}(\Theta_{\mathrm{C}})$ is the diagonal CMB covariance defined by the power spectrum $C_\ell(\Theta_{\mathrm{C}})$;
  - $\mathbf{M}$ is the non-diagonal noisy mask covariance matrix defined by

$$\mathbf{M}_{\ell m}^{\ell' m'} = \langle m_{\ell m}\, m^*_{\ell' m'} \rangle \simeq \sum_{\omega_i} \sigma_m^2(\omega_i) Y^*_{\ell m}(\omega_i)\, Y_{\ell' m'}(\omega_i)\, {\Omega_{\mathrm{pix}}}^2\,.$$

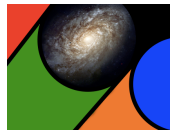

Bayesian analysis of Bianchi VII$_h$ cosmologies

Covariance

- Bianchi VII$_h$ templates can be computed accurately and rotated efficiently in harmonic space $\rightarrow$ consider harmonic space representation, where $\boldsymbol{d} = \{d_{\ell m}\}$ and $\boldsymbol{b}(\Theta_{\mathrm{B}}) = \{b_{\ell m}(\Theta_{\mathrm{B}})\}$.
- Partial-sky analysis that handles in harmonic space a mask applied in pixel space.
- Add masking noise in order to marginalise the pixel values of the data contained in the masked region, with variance for pixel i given by $\sigma_m^2(\omega_i)$.
- The covariance is then given by

$$\mathbf{X}(\Theta_{\mathrm{C}}) = \mathbf{C}(\Theta_{\mathrm{C}}) + \mathbf{M}\,,$$

where

  - $\mathbf{C}(\Theta_{\mathrm{C}})$ is the diagonal CMB covariance defined by the power spectrum $C_\ell(\Theta_{\mathrm{C}})$;
  - $\mathbf{M}$ is the non-diagonal noisy mask covariance matrix defined by

$$\mathbf{M}_{\ell m}^{\ell' m'} = \langle m_{\ell m}\, m^*_{\ell' m'} \rangle \simeq \sum_{\omega_i} \sigma_m^2(\omega_i) Y^*_{\ell m}(\omega_i)\, Y_{\ell' m'}(\omega_i)\, {\Omega_{\mathrm{pix}}}^2\,.$$

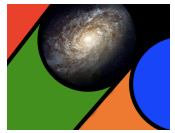

Bayesian analysis of Bianchi VII$_h$ cosmologies

Covariance

- Bianchi VII$_h$ templates can be computed accurately and rotated efficiently in harmonic space $\rightarrow$ consider harmonic space representation, where $\boldsymbol{d} = \{d_{\ell m}\}$ and $\boldsymbol{b}(\Theta_{\rm B}) = \{b_{\ell m}(\Theta_{\rm B})\}$.
- Partial-sky analysis that handles in harmonic space a mask applied in pixel space.
- Add masking noise in order to marginalise the pixel values of the data contained in the masked region, with variance for pixel i given by $\sigma^2_m(\omega_i)$.
- The covariance is then given by

$$\mathbf{X}(\Theta_{\rm C}) = \mathbf{C}(\Theta_{\rm C}) + \mathbf{M}\,,$$

where

- $\mathbf{C}(\Theta_{\rm C})$ is the diagonal CMB covariance defined by the power spectrum $C_\ell(\Theta_{\rm C})$;
- $\mathbf{M}$ is the non-diagonal noisy mask covariance matrix defined by

$$\mathbf{M}^{\ell' m'}_{\ell m} = \langle m_{\ell m}\, m^*_{\ell' m'} \rangle \simeq \sum_{\omega_i} \sigma^2_m(\omega_i) Y^*_{\ell m}(\omega_i)\, Y_{\ell' m'}(\omega_i)\, {\Omega_{\rm pix}}^2\,.$$

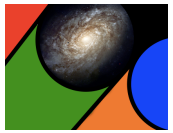

Bayesian analysis of Bianchi VII$_h$ cosmologies

Model selection

- Compute the Bayesian evidence to determine preferred model:

$$E = \mathrm{P}(\boldsymbol{d} \,|\, M) = \int \mathrm{d}\Theta \, \mathrm{P}(\boldsymbol{d} \,|\, \Theta, M) \, \mathrm{P}(\Theta \,|\, M) \; .$$

- Use MultiNest to compute the posteriors and evidences via nested sampling (Feroz & Hobson 2008, Feroz *et al.* 2009).
- Consider two models:
  - Flat-decoupled-Bianchi model: Θ_{C} and Θ_{B} fitted simultaneously but decoupled $\rightarrow$ phenomenological
  - Open-coupled-Bianchi model: Θ_{C} and Θ_{B} fitted simultaneously and coupled $\rightarrow$ physical

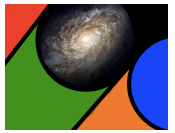

Bayesian analysis of Bianchi VII$_h$ cosmologies

Model selection

- Compute the Bayesian evidence to determine preferred model:

$$E = \mathrm{P}(\boldsymbol{d} \,|\, M) = \int \mathrm{d}\Theta \, \mathrm{P}(\boldsymbol{d} \,|\, \Theta, M) \, \mathrm{P}(\Theta \,|\, M) \; .$$

- Use MultiNest to compute the posteriors and evidences via nested sampling (Feroz & Hobson 2008, Feroz *et al.* 2009).
- Consider two models:
  - Flat-decoupled-Bianchi model: Θ_{C} and Θ_{B} fitted simultaneously but decoupled $\rightarrow$ phenomenological
  - Open-coupled-Bianchi model: Θ_{C} and Θ_{B} fitted simultaneously and coupled $\rightarrow$ physical

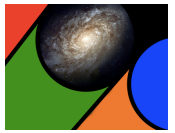

Bayesian analysis of Bianchi VII$_h$ cosmologies

Validation with simulations

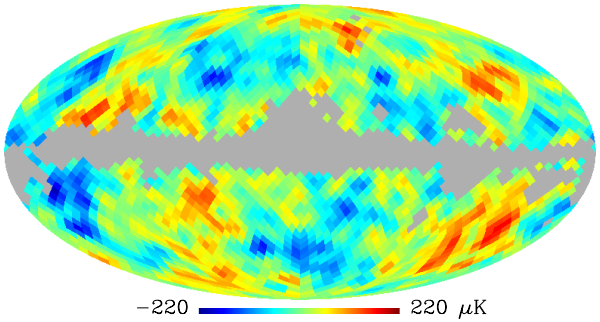

(a) CMB component

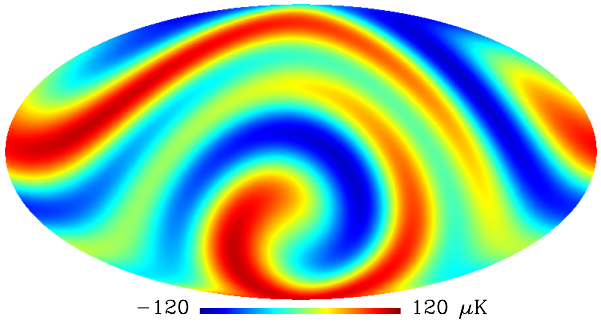

(b) Underlying Bianchi component

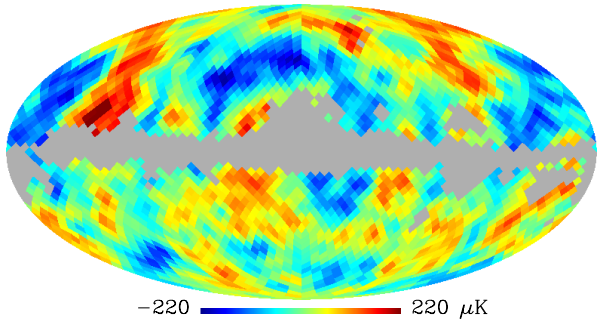

(c) CMB plus Bianchi components

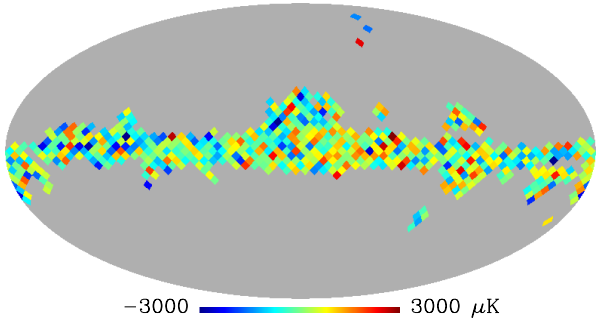

(d) Noisy mask realisation

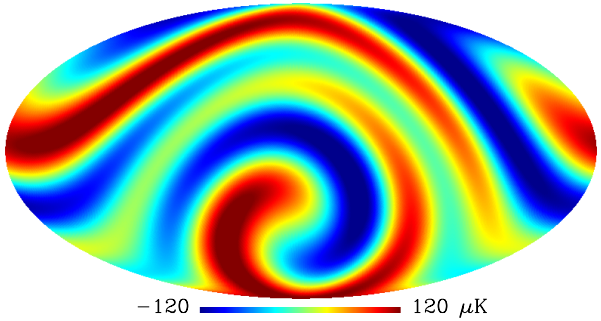

(e) Recovered Bianchi component

Figure: Partial-sky simulation with embedded Bianchi VII$_h$ component at $L = 32$.

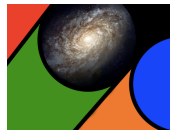

Bayesian analysis of Bianchi VII$_h$ cosmologies

Validation with simulations

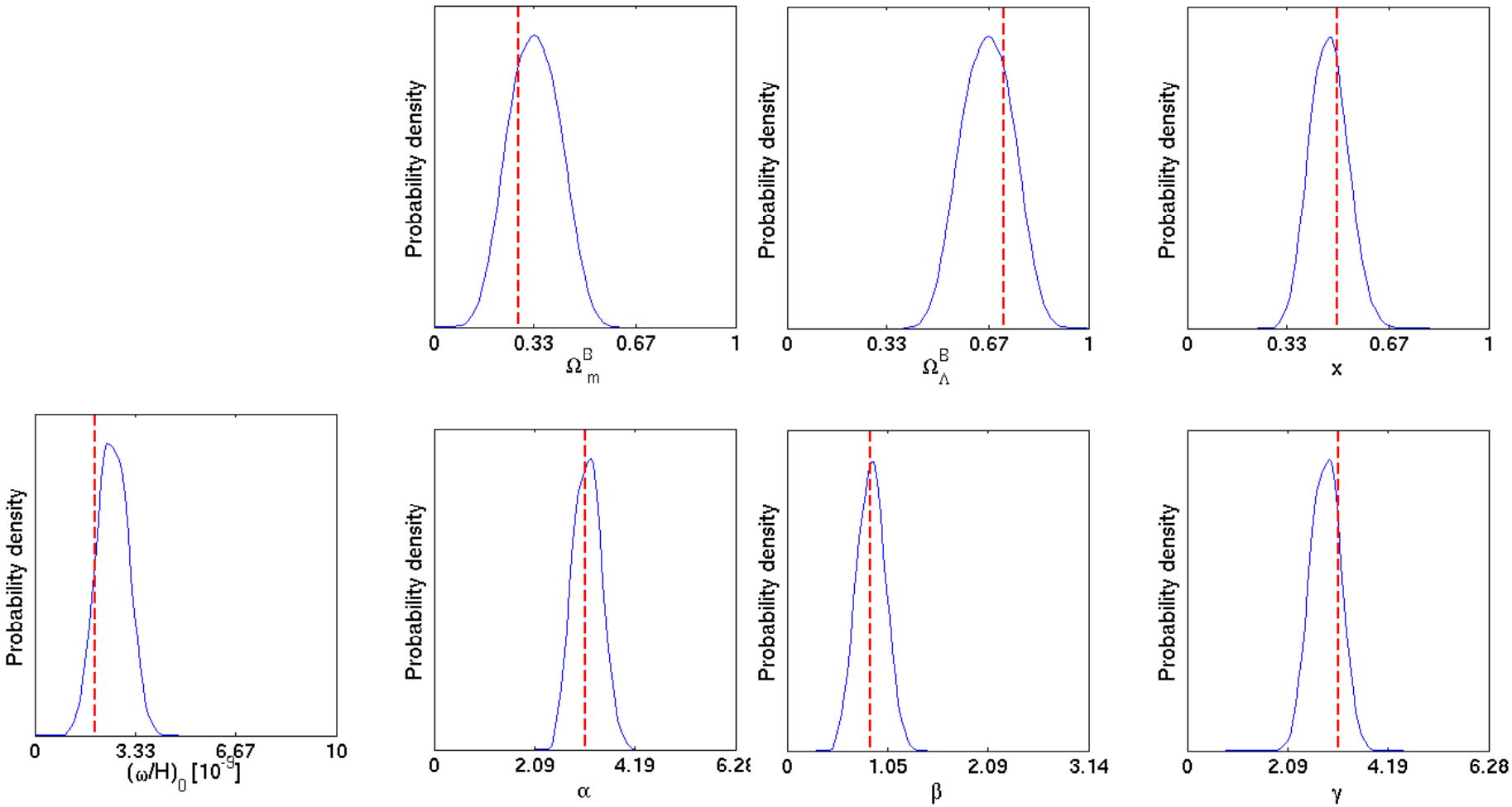

Figure: Marginalised posterior distributions recovered from partial-sky simulation at $L = 32$.

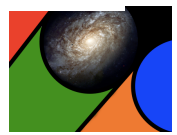

Planck results

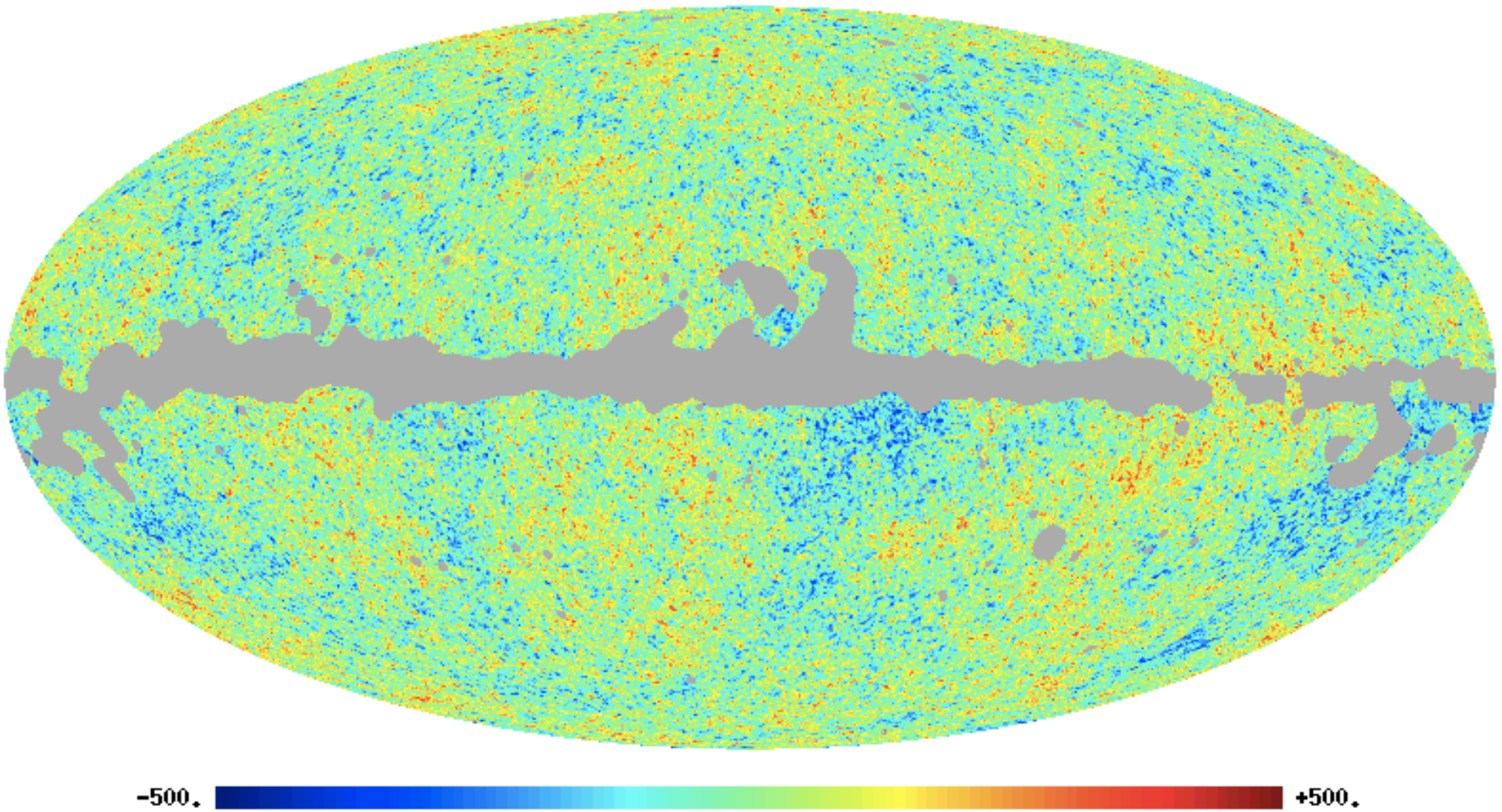

Figure: *Planck* SMICA component-separated data.

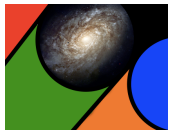

Planck results: flat-decoupled-Bianchi model

Bayesian evidence

Table: Bayes factor relative to equivalent ΛCDM model (positive favours Bianchi model).

Model	$\Delta \ln E$	
	SMICA	SEVEM
Flat-decoupled-Bianchi (left-handed)	2.8 ± 0.1	1.5 ± 0.1
Flat-decoupled-Bianchi (right-handed)	0.5 ± 0.1	0.5 ± 0.1

- On the Jeffreys (1961) scale, evidence for the inclusion of a Bianchi VII$_h$ component would be termed strong (significant) for SMICA (SEVEM) component-separated data.
- A log-Bayes factor of 2.8 corresponds to an odds ratio of approximately 1 in 16.

Planck data favour the inclusion of a phenomenological Bianchi VII$_h$ component!

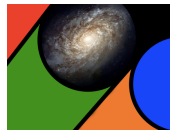

Planck results: flat-decoupled-Bianchi model

Best-fit Bianchi component

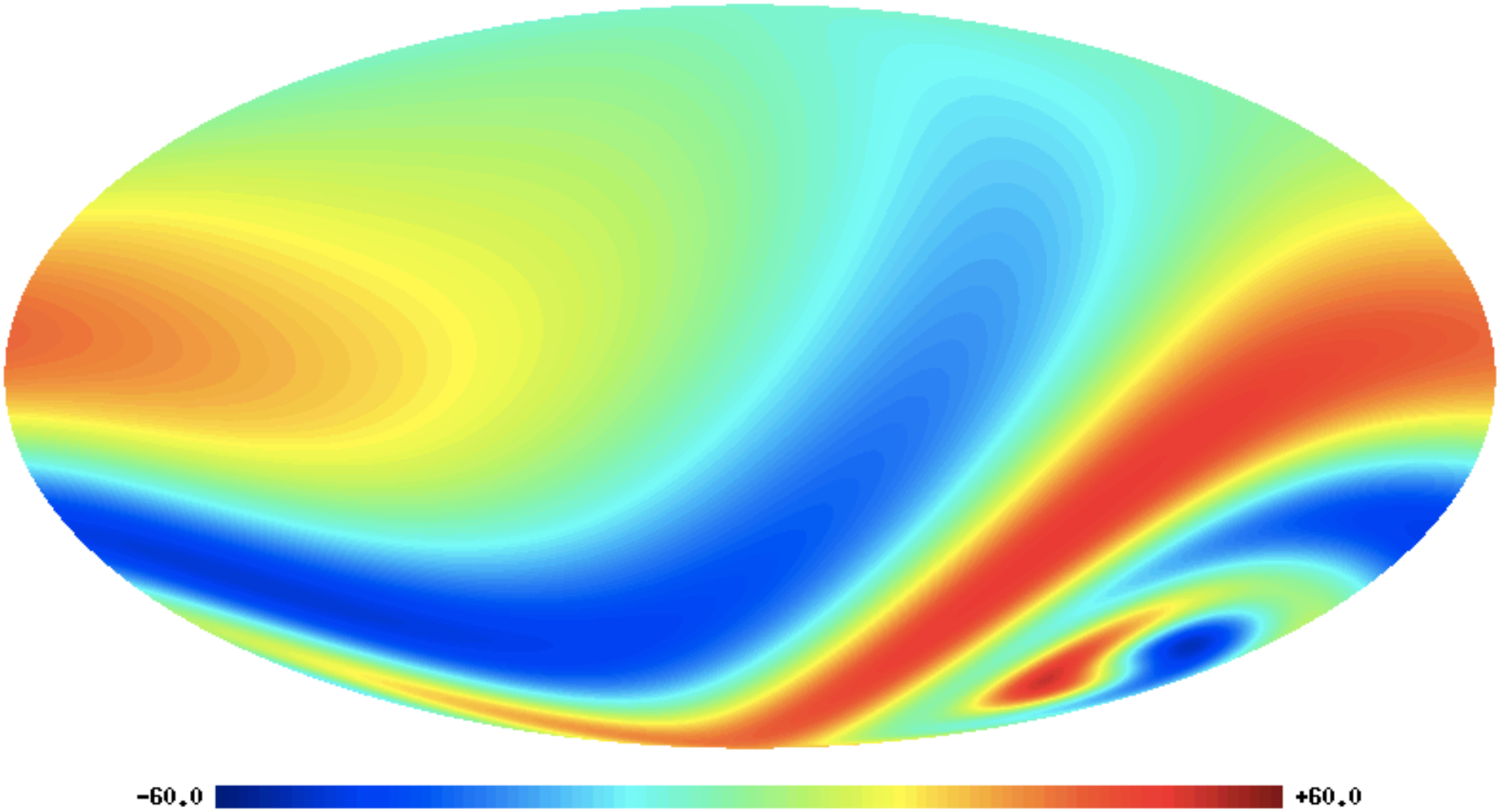

Figure: Best-fit template of flat-decoupled-Bianchi VII_h model found in *Planck* SMICA component-separated data.

Planck results: flat-decoupled-Bianchi model

BUT the flat-Bianchi-decoupled model is phenomenological and **not physical!**

Parameter estimates are not consistent with concordance cosmology.

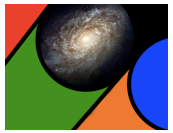

Planck results: open-coupled-Bianchi model

Bayesian evidence

Table: Bayes factor relative to equivalent ΛCDM model (positive favours Bianchi model).

Model	$\Delta \ln E$	
	SMICA	SEVEM
Open-coupled-Bianchi (left-handed)	0.0 ± 0.1	0.0 ± 0.1
Open-coupled-Bianchi (right-handed)	-0.4 ± 0.1	-0.4 ± 0.1

- In the physical setting where the standard cosmological and Bianchi parameters are coupled,

  Planck data do not favour the inclusion of a Bianchi VII_h component.

- Find no evidence for Bianchi VII_h cosmologies and constrain vorticity to:

$$(\omega/H)_0 < 8.1 \times 10^{-10}$$

95% confidence level

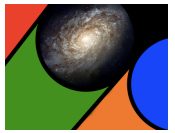

Planck results: open-coupled-Bianchi model

Bayesian evidence

Table: Bayes factor relative to equivalent ΛCDM model (positive favours Bianchi model).

Model	$\Delta \ln E$	
	SMICA	SEVEM
Open-coupled-Bianchi (left-handed)	0.0 ± 0.1	0.0 ± 0.1
Open-coupled-Bianchi (right-handed)	-0.4 ± 0.1	-0.4 ± 0.1

- In the physical setting where the standard cosmological and Bianchi parameters are coupled,

  Planck data do not favour the inclusion of a Bianchi VII_h component.

- Find no evidence for Bianchi VII_h cosmologies and constrain vorticity to:

$$(\omega/H)_0 < 8.1 \times 10^{-10}$$

95% confidence level

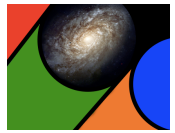

Summary

We have entered an era of precision cosmology.

Thanks to large and precise cosmological observations and robust signal and image processing techniques.

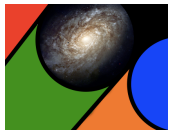

Summary

We have entered an era of precision cosmology.

Thanks to large and precise cosmological observations and robust signal and image processing techniques.

BUT... many outstanding questions remain!

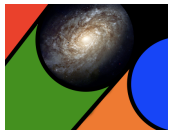

Summary

We have entered an era of precision cosmology.

Thanks to large and precise cosmological observations and robust signal and image processing techniques.

BUT... many outstanding questions remain!

Your Universe needs YOU!

PhD and postdoc opportunities at UCL.

For more information see
`http://www.jasonmcewen.org/opportunities.html`